© 2020. Published by The Company of Biologists Ltd | Development (2020) 147, dev181560. doi:10.1242/dev.181560

RESEARCH ARTICLE

Cyp26b1 is an essential regulator of distal airway epithelial differentiation during lung development

Edward Daniel*, Haley R. Barlow*, Gabrielle I. Sutton, Xiaowu Gu, Yadanar Htike, Mitzy A. Cowdin and Ondine Cleaver‡

ABSTRACT

Proper organ development depends on coordinated communication between multiple cell types. Retinoic acid (RA) is an autocrine and paracrine signaling molecule essential for the development of most organs, including the lung. Despite extensive work detailing effects of RA deficiency in early lung morphogenesis, little is known about how RA regulates late gestational lung maturation. Here, we investigate the role of the RA catabolizing protein Cyp26b1 in the lung. Cyp26b1 is highly enriched in lung endothelial cells (ECs) throughout development. We find that loss of Cyp26b1 leads to reduction of alveolar type 1 cells, failure of alveolar inflation and early postnatal lethality in mouse. Furthermore, we observe expansion of distal epithelial progenitors, but no appreciable changes in proximal airways, ECs or stromal populations. Exogenous administration of RA during late gestation partially mimics these defects; however, transcriptional analyses comparing Cyp26b1$^{-/-}$ with RA-treated lungs reveal overlapping, but distinct, responses. These data suggest that defects observed in Cyp26b1$^{-/-}$ lungs are caused by both RA-dependent and RA-independent mechanisms. This work reports crucial cellular crosstalk during lung development involving Cyp26b1-expressing endothelium and identifies a novel RA modulator in lung development.

KEY WORDS: Lung, Cyp26b1, Epithelium, Retinoic acid, Endothelial cell, Epithelial cell, Mouse

INTRODUCTION

Organogenesis requires tightly orchestrated crosstalk between endothelial cells (ECs), epithelial cells and stromal cells to form a mature and functional organ. These cell types communicate with one another using a multitude of distinct signaling pathways that must be activated at the right place and time to promote proper development (Kraus and Grapin-Botton, 2012; Rankin et al., 2018). Coordination is central to development, and aberrations in any one step of this multistep process can have catastrophic developmental consequences. Despite this, there is still much to learn concerning the mechanisms that underlie spatiotemporal control of developmental signaling cues over the course of organogenesis.

Lung development begins at embryonic day (E)9.0 with specification of lung progenitors along the ventral side of the anterior foregut endoderm (Herriges and Morrisey, 2014; Shi et al., 2009; Warburton et al., 2010). These progenitors undergo initial bud formation, followed by highly stereotyped and hierarchical branching to form the lung airway tree (Metzger et al., 2008). During this process, the lung epithelium segregates into two separate groups: the distal airways, which give rise to alveoli where gas exchange occurs, and proximal airways, which form the bronchi and bronchioles. By E16.5, the distal airways begin to differentiate into pre-alveolar structures called canaliculi and saccules, consisting of alveolar type 2 (AT2) surfactant-producing cells and alveolar type 1 (AT1) gas-exchanging cells. These structures mediate gas exchange in neonates until full alveolarization occurs postnatally (Herriges and Morrisey, 2014; Morrisey and Hogan, 2010). Understanding the drivers of this process has the potential to impact human health, as premature infants are at an increased risk for developing respiratory distress syndrome (RDS) because of immaturity of distal airways, with a mortality rate as high as 50% (Gallacher et al., 2016).

Retinoic acid (RA) is an essential signaling molecule that exhibits highly regulated spatiotemporal control during embryogenesis. RA directs cell fate by binding to the RAR and RXR family of nuclear receptors to direct changes in gene transcription. RA is derived from vitamin A (retinol) consumed in our diet. Vitamin A is first dehydrogenated to form retinaldehyde, then retinaldehyde is further dehydrogenated by Raldh1-Raldh3 (also known as Aldh1a1-Aldh1a3) to form the active forms of RA, with all-trans retinoic acid (atRA) being the most abundant and potent form. Once synthesized, RA can act as an autocrine signal or can diffuse to nearby cells as a paracrine signal, forming a local gradient (Duester, 2008). Antagonizing RA signaling is the Cyp26 family of P450 enzymes, consisting of Cyp26a1, Cyp26b1 and Cyp26c1. These enzymes metabolize RA into inactive forms. The expression of these genes requires precise control, as genetic or pharmacologic manipulations resulting in RA excess or deficiency drastically affect nearly every developing organ (Duester, 2008; Rhinn and Dolle, 2012).

Lung development and maturation are known to require proper spatiotemporal regulation of RA signaling. Mice lacking Raldh2 or fed on a vitamin A-deficient diet fail to initiate lung formation, resulting in lung agenesis (Wang et al., 2006; Wilson et al., 1953). In the initial lung bud, RA activates the Wnt cascade via Shh, and inhibits TGF-β signaling (Chen et al., 2010, 2007; Rankin et al., 2016, 2018). Together, this leads to upregulation of Fgf10, a crucial factor necessary for lung bud formation and branching (Desai et al., 2004; Park et al., 1998; Wang et al., 2006). Once lung branching is initiated, RA activity decreases until birth, allowing for proper epithelial branching and distal airway differentiation. Culturing E12.5 lung explants with RA leads to a reduction in branching due to decreased Fgf10 (Malpel et al., 2000). Likewise, forcing increased RA signaling in distal lung epithelial cells through a

Department of Molecular Biology and Center for Regenerative Science and Medicine, University of Texas Southwestern Medical Center, Dallas, TX 75390, USA.
*These authors contributed equally to this work

‡Author for correspondence (ondine.cleaver@utsouthwestern.edu)

E.D., 0000-0003-3208-9655; H.R.B., 0000-0003-3414-4574; G.I.S., 0000-0002-9424-9629; X.G., 0000-0003-2266-5516; M.A.C., 0000-0003-0549-2473; O.C., 0000-0003-2454-6641

Received 25 June 2019; Accepted 23 January 2020

Development (2020) 147, dev181560. doi:10.1242/dev.181560

constitutively active RAR *in vivo* prevents distal saccule differentiation (Wongtrakool et al., 2003). Lastly, a third, separate role for RA occurs postnatally during alveolar maturation. At this stage, RA promotes increased alveolar septation, alveolar number and alveolar surface area (Massaro and Massaro, 1996, 2000; Massaro et al., 2003; McGowan et al., 2000). Taken together, these studies indicate that RA is essential for the regulation of several distinct steps during lung development in a highly temporally defined manner. However, the role of RA signaling in lung development during late gestation (later than E15.5) is not fully understood.

Although RA signaling has been shown to regulate specification and differentiation of lung cell types, the role of RA-catabolizing Cyp26 enzymes during lung development remains unknown. Cyp26a1 is expressed in the epithelium during early stages of lung branching, but its expression diminishes and is absent by E16.5 when distal epithelial differentiation begins (Malpel et al., 2000). On the other hand, Cyp26b1 is expressed in non-epithelial cells at E18.5 (Abu-Abed et al., 2002). Deletion of Cyp26b1 leads to neonatal lethality, which was suggested to occur from pulmonary dysfunction, although this phenotype was not characterized further (Yashiro et al., 2004). These data suggest that Cyp26b1 may be required in the lung during late gestation to reduce RA signaling and promote proper distal epithelial differentiation in a paracrine manner.

Here, we identify a crucial role for Cyp26b1 during lung organogenesis. Cyp26b1 is highly enriched in lung ECs throughout development, and loss of Cyp26b1 results in a delay in the formation of distal airways in late gestation. E18.5 Cyp26b1$^{-/-}$ lungs exhibit increased cellular density and contain an expansion of a distal tip progenitor population at the expense of mature gas-exchanging AT1 cells. Exogenous administration of atRA during late gestation phenocopies loss of Cyp26b1, suggesting that the phenotype is due, at least in part, to excess RA. However, transcriptional analyses of atRA-treated and Cyp26b1$^{-/-}$ lungs reveal only partially overlapping responses, suggesting RA-independent signaling pathways downstream of Cyp26b1 in the lung. These findings identify Cyp26b1 as a novel endothelial modulator of RA activity in the developing lung and reveal RA-independent functions during lung development.

RESULTS

Cyp26b1 is highly enriched in lung and kidney ECs

We have previously identified *Cyp26b1* as an endothelial-enriched gene in embryonic organs, including kidney and lung, using RNA-seq (Daniel et al., 2018). *Cyp26b1* was expressed in the mesenchyme of these embryonic organs, suggesting possible lung EC enrichment (Abu-Abed et al., 2002) (Fig. 1). To differentiate between the two major cell types resident in the lung mesenchyme – lung ECs and stromal cells – we assessed *Cyp26b1* expression in publicly available single cell (sc)RNA-seq datasets of fetal, early postnatal and adult tissues. These studies confirmed elevated expression of *Cyp26b1* in ECs compared with non-ECs (Fig. S1; Du et al., 2015, 2017; Guo et al., 2019; Lindstrom et al., 2018; Sabbagh et al., 2018; Tabula Muris et al., 2018).

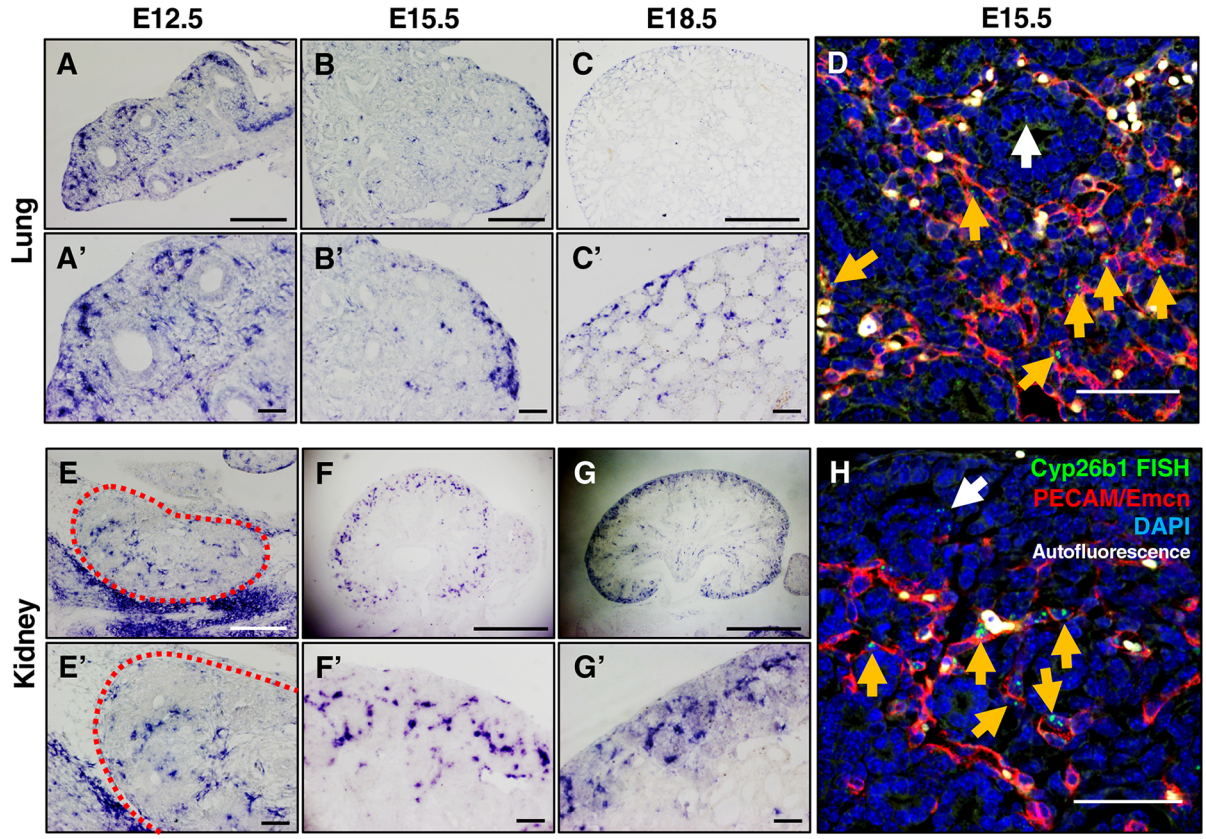

Fig. 1. Cyp26b1 is highly enriched in lung and kidney endothelial cells during development. (A-H) ISH of *Cyp26b1* in the lung (A-D) and kidney (E-H) at E12.5 (A,A′,E,E′), E15.5 (B,B′,D,F,F′,H) and E18.5 (C,C′,G,G′). Magnifications for chromogenic assays are shown. Red dotted outline (E,E′) delineates the E12.5 kidney. D and H show FISH for Cyp26b1 (green) co-stained with PECAM and Emcn (red) to mark ECs. Orange arrows, Cyp26b1^{+} punctae in PECAM/Emcn^{+} ECs; white arrow, Cyp26b1^{+} puncta in non-EC cells. Scale bars: 200 µm (A,B,E); 100 µm (A′,B′,C′,E′,F′,G′); 500 µm (C,F,G); 50 µm (D,H).

Development (2020) 147, dev181560. doi:10.1242/dev.181560

To validate these data, we performed *in situ* hybridization (ISH) for *Cyp26b1* in E12.5, E15.5 and E18.5 embryonic organs. These experiments revealed an endothelial-like expression pattern in both lung and kidney (Fig. 1A-C′,E-G′). Consistent with previously published data, *Cyp26b1* was also expressed in the developing limbs, the face and palate, the tongue, the hindbrain, intersomitic regions along the back, in endocardial cushions extending into the great vessels and the epicardium (Fig. S2A-E′) (Abu-Abed et al., 2002; Spoorendonk et al., 2008). By E15.5, *Cyp26b1* expression in lungs was restricted to the ECs in the distal periphery (Fig. 1B-C′). Likewise, *Cyp26b1* expression in the kidney became restricted to ECs in the outer cortex (Fig. 1F-G′). We validated EC specificity of *Cyp26b1* using fluorescent *in situ* hybridization (FISH) analysis and co-staining with the endothelial markers PECAM and endomucin (Emcn) (Fig. 1D,H). Further, *Cyp26b1* FISH co-stained with Lyve1 revealed that *Cyp26b1* is also expressed in lymphatic endothelium in the lung (Fig. S2F-F′). Of note, *Cyp26b1*$^{+}$ punctae were observed in some epithelial and stromal regions, but at much lower levels compared with ECs (white arrows). Thus, *Cyp26b1* expression is highly enriched in lung and kidney ECs throughout development.

Generation of Cyp26b1 null mice using CRISPR/Cas9

Previous work using a Cyp26b1 germline deficient mouse model showed that Cyp26b1 null mutants die shortly after birth because of respiratory distress (Yashiro et al., 2004). We generated two independently derived Cyp26b1-null mouse models using CRISPR/Cas9 to further explore these defects. Our first model contained an in-frame 2.6 kb deletion from exon 3 to exon 6 (referred to as Cyp26b1^{-}) and the second contained a 10 bp deletion in exon 3 leading to a frame-shift mutation (referred to as Cyp26b1$^{\Delta 10}$). Both Cyp26b1$^{-/-}$ and Cyp26b1$^{\Delta 10/\Delta 10}$ embryos exhibited many of the same developmental defects as previously described, including limb defects, craniofacial abnormalities, micrognathia, cleft palate, skin abnormalities and spleen hypoplasia, although edema and hemorrhages were not observed at this stage as previously described (Fig. 2A,B) (Bowles et al., 2014; Dranse et al., 2011; Lenti et al., 2016; Okano et al., 2012a,b; Yashiro et al., 2004). In addition, Cyp26b1$^{-/-}$ mice died shortly after birth and exhibited signs of respiratory distress, including air hunger, mirroring the previously generated null model. These observations and previously published data both support a role for Cyp26b1 in regulating lung development.

Cyp26b1 null mice exhibit lung defects

To further explore how loss of Cyp26b1 affects lung development in late gestation, we analyzed Cyp26b1$^{+/+}$ and Cyp26b1$^{-/-}$ lungs at E18.5, immediately before birth. E18.5 Cyp26b1$^{-/-}$ lungs were smaller but with grossly normal lobation (Fig. 2C,D). Interestingly, Cyp26b1$^{-/-}$ lungs had decreased distal airspaces compared with control littermates (Fig. 2C′,D′). In tissue sections, Cyp26b1$^{-/-}$ lungs appeared to be hypercellular, with increased septal wall thickness and smaller airspaces, although the total number of airspaces was not different (Fig. 2E-K). To determine whether this phenotype was due to an increase in total cell number or due to a partial failure of alveologenesis, we measured the wet and dry weights of these lungs. Measurements of the wet and dry weight standardized to total body weight confirmed that Cyp26b1$^{-/-}$ lungs are smaller without an increase in total mass (Fig. 2L-N). These data suggest that the phenotype in Cyp26b1$^{-/-}$ lungs is due to an increase in the density of cells within the lung and not due to increased total number of cells.

Cyp26b1 is necessary for distal epithelial maturation

Based on these gross changes in epithelial morphology, we asked whether distal epithelial specification was affected in E18.5 Cyp26b1$^{-/-}$ lungs. We first assessed changes in the frequency of AT1 and AT2 cells. Immunofluorescent (IF) stains for the AT1 cell marker HOPX revealed a significant decrease in AT1 cells upon loss of Cyp26b1 (Fig. 3A-C). Of note, Cyp26b1$^{-/-}$ lungs contain a lower proportion of AT1 cells after standardizing for the increased number of DAPI^{+} cells per given area. Staining for the additional AT1 markers podoplanin (Pdpn) and aquaporin 5 (Aqp5) confirmed the reduction in distal airway cells in the mutants (Fig. S3A-D). IF stains for the AT2 marker pro-surfactant protein C (proSP-C; Sftpc) at E18.5 revealed that Cyp26b1$^{-/-}$ lungs contain an increase in AT2 cells compared with control littermates (Fig. 3D-F). Because proSP-C is not exclusively expressed in AT2 cells during development (Frank et al., 2019), we repeated the analysis using the AT2 cell-specific marker lysosomal-associated membrane protein 3 (Lamp3 or DC-Lamp). Quantification of AT2 cells using Lamp3 demonstrated a similar increase in Lamp3^{+} AT2 cells compared with proSP-C^{+} AT2 cells in Cyp26b1$^{-/-}$ lungs, with the vast majority of AT2 cells expressing both proteins (Fig. S3E-J). To determine whether this increase in AT2 cells could be the result of a general increase in the total number of epithelial cells, we stained E18.5 lungs for pan-epithelial nuclear marker Nkx2.1. Quantification revealed no change in the total number of distal epithelial cells (Fig. S3K-M). These data show that there is no change in total distal epithelial cell number, but rather a change in the proportion of AT1 and AT2 cells.

These apparent changes in epithelial differentiation led us to ask whether there were changes in epithelial AT1 or AT2 progenitor populations. Sox9^{+} cells located at the tips of the distal epithelium are primarily fated to become AT2 cells (Frank et al., 2019; Rockich et al., 2013). These cells first express both Sox9 and proSP-C/Lamp3, then become exclusively proSP-C/Lamp3-positive as they differentiate into mature AT2 cells (Rockich et al., 2013). We observed an increase in Sox9^{+} distal epithelial progenitor cells in Cyp26b1$^{-/-}$ lungs (Fig. 3G-I). To determine whether the increase in Sox9^{+} and proSP-C^{+}/Lamp3^{+} cells in Cyp26b1$^{-/-}$ lungs represents an increase in two distinct populations or in the same distal tip progenitor population, we co-stained E18.5 lungs with both Sox9 and Lamp3. Quantification of these populations revealed an expansion in only Sox9^{+}/Lamp3^{+} cells, with no change in Sox9^{+}/Lamp3^{-} or Sox9^{-}/Lamp3^{+} cells (Fig. 3J and Fig. S3N,O). We sought to further validate the IF stains with western blot and qRT-PCR analyses on E18.5 tissues. Western blot analyses demonstrated a decrease in the AT1 cell marker Aqp5 and an increase in proSP-C protein levels, validating the IF data (Fig. S3P). Likewise, qRT-PCR for the AT1 cell markers *Aqp5*, *Pdpn*, *HOPX* and *Ager* (*RAGE*) revealed ∼40% decrease in mRNA abundance in Cyp26b1$^{-/-}$ lungs; however, in contrast to the IF analysis, *Sox9*, *Sftpc* and *Lamp3* mRNA levels were not significantly altered (Fig. S3Q).

Defects in lung development are not due to off-target CRISPR lesions

Because our Cyp26b1 mutant mice were generated using CRISPR/Cas9-mediated mutagenesis, we considered the possibility that there may be off-target effects contributing to these phenotypes. These off-target effects can be eliminated by crossing two independently derived null alleles to create compound heterozygotes. Any phenotypes observed in compound heterozygotes can then be fully

Development (2020) 147, dev181560. doi:10.1242/dev.181560

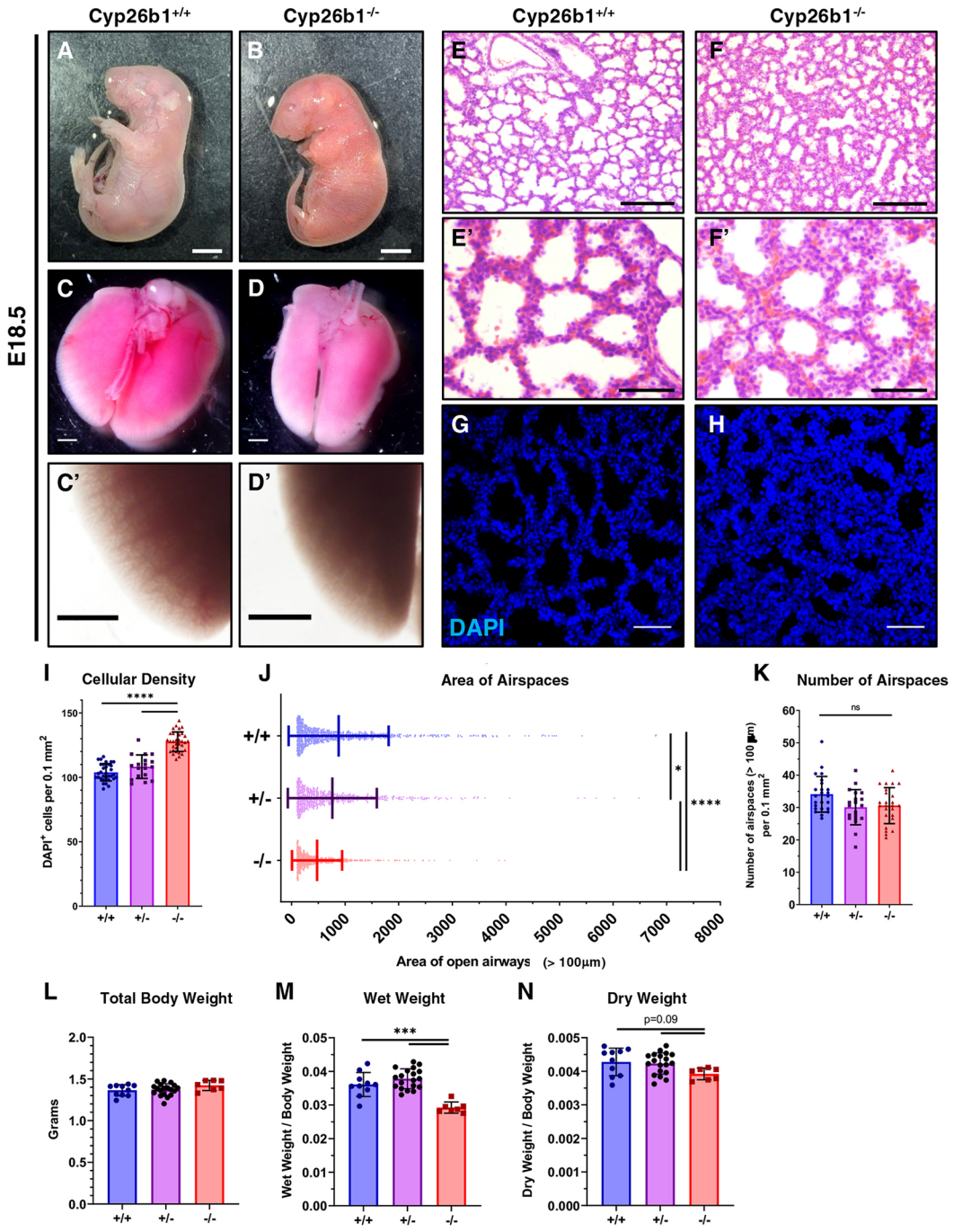

Fig. 2. Cyp26b1 mutant lungs exhibit increased cellular density and decreased airspaces at late gestation. (A,B) E18.5 Cyp26b1$^{+/+}$ and Cyp26b1$^{-/-}$ embryos at dissection. (C,D′) Lungs from Cyp26b1$^{+/+}$ and Cyp26b1$^{-/-}$ E18.5 embryos. C′ and D′ show magnified areas of lungs in C and D, respectively, with backlight to highlight loss of distal airspaces in Cyp26b1$^{-/-}$ lungs. (E-F′) H&E stain of E18.5 Cyp26b1$^{+/+}$ and Cyp26b1$^{-/-}$ lungs at 10× (E,F) and 40× (E′,F′) magnification. (G,H) Representative images of DAPI stains used in quantifications for I-K. (I) Number of DAPI^{+} cells per 0.1 mm^2. *n*=5 (+/+, –/–) and 3 (+/–) with six random views per sample. (J) Scatter plots depicting area of open airspaces (>100 μm^2) in Cyp26b1$^{+/+}$, Cyp26b1$^{+/-}$ and Cyp26b1$^{-/-}$ lungs. *n*=4 (+/+, –/–) and 3 (+/–) with six random views per sample. (K) The total number of open airspaces (>100 μm^2) per 0.1 mm^2. *n*=4 (+/+, –/–) and 3 (+/–) with six random views per sample. (L) Total body weight of E18.5 embryos. (M) Weight of lungs immediately after dissection (wet) relative to total body weight in E18.5 embryos. (N) Weight of lungs after drying relative to total body weight in E18.5 embryos. *n*=10 (+/+), 19 (+/–) and 7 (–/–). Data are mean±s.d. **P*<0.05, ****P*<0.001, *****P*<0.0001. Significance for all experiments was determined using one-way ANOVA with Tukey multiple comparison test. ns, not significant. Scale bars: 5 mm (A,B); 1 mm (C-D′); 500 μm (E,F); 50 μm (E′,F′,H).

attributed to loss of the target gene. We generated compound heterozygotes of Cyp26b1 by crossing the Cyp26b1^{-} allele with the Cyp26b1$^{\Delta 10}$ allele. E18.5 Cyp26b1$^{-/\Delta 10}$ embryos completely phenocopied Cyp26b1$^{-/-}$ embryos. When analyzed similarly to the Cyp26b1$^{-/-}$ embryos, E18.5 Cyp26b1$^{-/\Delta 10}$ embryos displayed the same gross developmental defects, decreased distal airspaces, increased cellularity and increased relative numbers of distal tip epithelial progenitors (Sox9^{+}) and AT2 cells (Fig. S4).

Development (2020) 147, dev181560. doi:10.1242/dev.181560

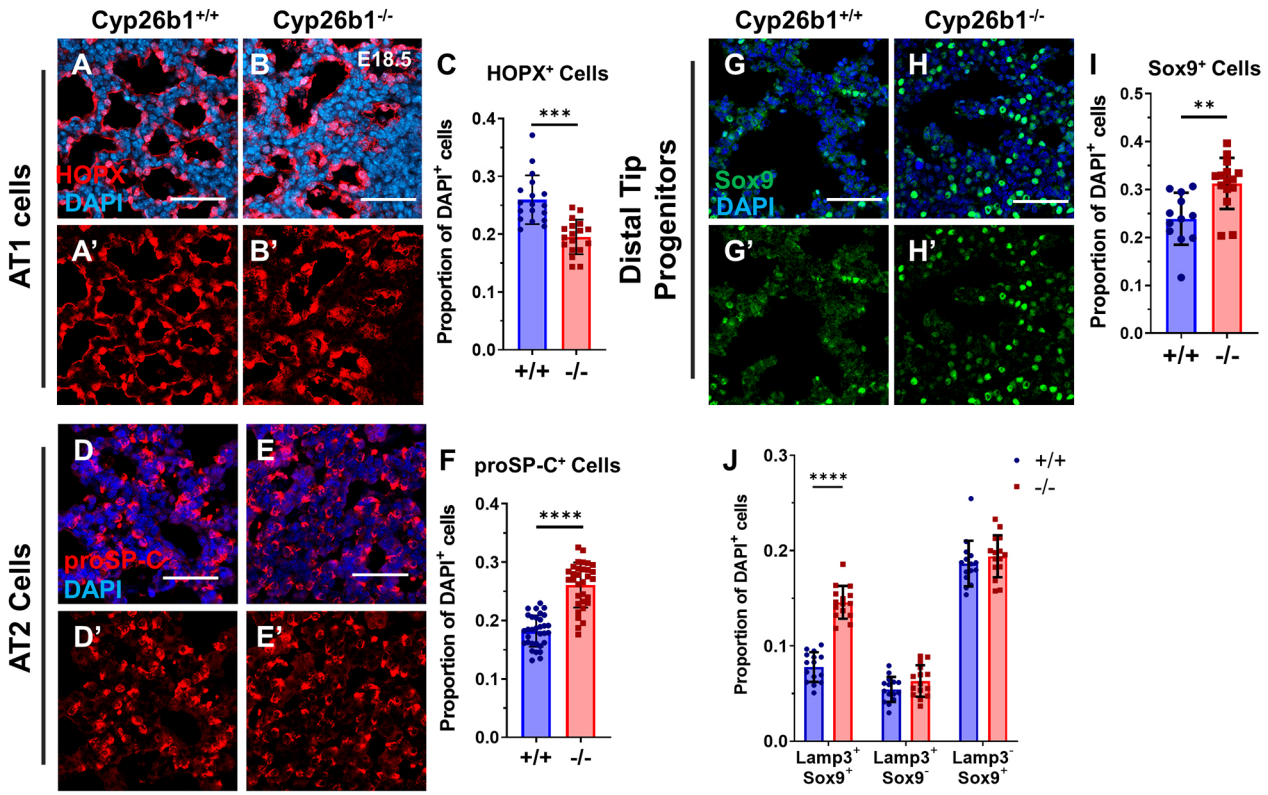

Fig. 3. Distal tip epithelial progenitors are expanded at the expense of AT1 cells in Cyp26b1$^{-/-}$ lungs. (A-C) IF stain for the AT1 marker HOPX (A-B′) and quantification of cell counts (C). *n*=3 biological replicates with six random views per sample. (D-F) IF stain for the AT2 marker proSP-C (D-E′) and quantification of cell counts (F). *n*=5 biological replicates with six random views per sample. (G-I) IF stain for the distal progenitor cell marker Sox9 (G-H′) and quantification of cell counts (I). *n*=3 biological replicates with six random views per sample. (J) Quantification of Lamp3/Sox9 double positive cells (first set), Lamp3 single positive cells (second set) and Sox9 single positive cells (third set) as a proportion of DAPI$^+$ cells. *n*=3 biological replicates with five random views per sample. Note that the quantifications in C, F, I, and J are standardized to the total number of DAPI$^+$ cells. Data are mean±s.d. ***P*<0.01, ****P*<0.001, *****P*<0.0001. Significance determined with unpaired Student's *t*-test (C,F,I) and two-way ANOVA with Sidak multiple comparison test (J). Scale bars: 50 µm.

Proximal airways, stroma, endothelia and lymphatics of Cyp26b1$^{-/-}$ lungs are grossly normal

After confirming that observed changes in distal epithelial development were not due to off-target effects of CRISPR/Cas9, we assayed for changes in other populations in Cyp26b1$^{-/-}$ lungs. Proximal airways in Cyp26b1$^{-/-}$ lungs appeared to be unaffected as there were no appreciable differences in gross morphology or in the localization of CCSP$^+$ (Scgb1a1) secretory cells (Clara cells), Foxj1$^+$ ciliated cells (bronchial in embryonic lungs) or Sox2$^+$ proximal epithelial cells (Fig. S5A-D′). CCSP$^+$/Sca-1$^+$ (Ly6a) bronchioalveolar stem cells (BASCs) are a stem cell population that reside at the transition between proximal and distal airways and can give rise to distal epithelium in the adult during lung regeneration (Kim et al., 2005; Lee et al., 2014). Analysis of BASCs by flow cytometry revealed no differences in this population at any stage in late gestation (Fig. S5E,F).

As ECs are closely associated with many different cell types in the lung, we set out to determine whether there were defects in cell types other than the distal epithelium. We analyzed Pdgfr-α and Pdgfr-β stromal populations using IF at E18.5 and did not observe any striking differences. Flow cytometry analysis of Pdgfr-α cells confirmed that there was no significant difference in the stromal makeup of Cyp26b1$^{-/-}$ lungs at E18.5 (Fig. S6A-C). Several groups have established a link between RA signaling and proper vascular formation in the heart through directing proper vascular smooth muscle cell differentiation and association of the vasculature with these smooth muscle cells (Braitsch et al., 2012; Wang et al., 2018; Xiao et al., 2018). Co-stains for VE-Cad (Cdh5) and Pdgfr-β to mark the ECs and pericytes, respectively, did not reveal any differences in EC-pericyte coupling (Fig. S6D-E′). Despite the fact that Cyp26b1 is highly enriched in ECs and also observed in lymphatic ECs, we did not observe gross defects in vascular organization (Fig. S6F-G′). We also observed no obvious differences in arterial, venous or lymphatic development (Fig. S6H-K′). Lastly, RA has been shown to direct the differentiation of stromal-derived smooth muscle cells during lung organogenesis (Chen et al., 2014). Analysis using the marker Sm22a (protein product of *Tagln*) revealed that smooth muscle cells around both airways and vessels were not appreciably altered in Cyp26b1$^{-/-}$ lungs (Fig. S6L-M′). These data demonstrate that formation of the vasculature, stroma and associated lineages is not grossly affected in Cyp26b1$^{-/-}$ lungs.

Cyp26b1 is required for distal airway morphogenesis in late gestation

Our results show that AT1 and AT2 cell differentiation is altered in Cyp26b1$^{-/-}$ lungs at the end of gestation. To determine when this phenotype arises, we analyzed earlier stages of lung development. Distal airway terminal differentiation begins at E16.5 when the columnar epithelium undergoes dramatic cell-shape changes that lead to lumen expansion and formation of distal saccules for gas exchange (Herriges and Morrisey, 2014; Shi et al., 2009; Warburton et al., 2010). Consistent with this timeline, Cyp26b1$^{-/-}$ lungs begin to show gross morphological defects beginning at E16.5,

Development (2020) 147, dev181560. doi:10.1242/dev.181560

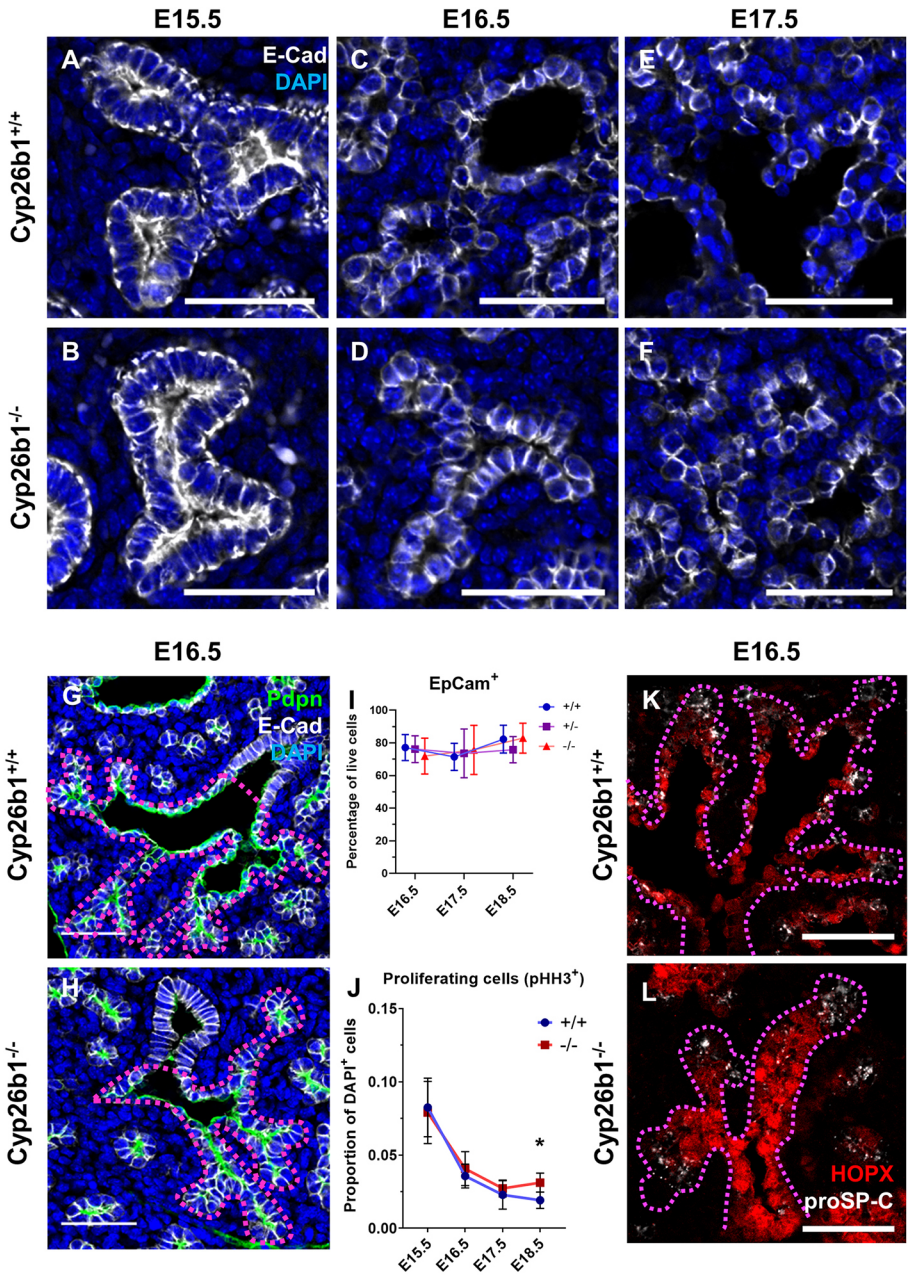

Fig. 4. Defects in epithelial morphogenesis in Cyp26b1$^{-/-}$ lungs arise at E16.5. (A-F) IF stains for E-Cad (white) to mark the epithelial structure at E15.5 (A,B), E16.5 (C,D) and E17.5 (E,F). (G,H) Proximal to distal epithelial transition in E16.5 lungs stained with Pdpn (green) and E-Cad (white). Magenta dotted outlines mark distal epithelial tree extending from the terminal bronchiole. (I) Flow cytometry analysis of EpCam^{+}/CD31^{-}/CD45^{-} cells in E16.5-E18.5 lungs. *n*=9 (E16.5 +/+), 4 (E16.5 ±, E18.5 –/–), 3 (E16.5 –/–), 10 (E17.5 +/+, E17.5 ±), 6 (E17.5 –/–, E18.5 ±) and 5 (E18.5 +/+). (J) Quantification of pHH3^{+} cells as a proportion of DAPI^{+} cells from E15.5-E18.5 based on IF sections. *n*=3 with six random views per sample. (K-L) Distal epithelial tree in E16.5 lungs stained with E-Cad (green), HOPX (red) and proSP-C (white). Magenta dotted outlines mark distal epithelial tree. Data are mean±s.d. *P<0.05. Significance was determined using two-way ANOVA with Sidak multiple comparison test. Scale bars: 50 µm.

characterized by increased cellular density and decreased distal airspace formation (Fig. S7). During distal epithelial differentiation, subsets of epithelial cells marked by E-cadherin (E-Cad; Cdh1) undergo morphogenetic changes from a columnar, glandular-like structure (E15.5) to a flattened, or squamous, morphology for AT1 cells and a rounded morphology for AT2 cells (E17.5) (Fig. 4A,C,E). In Cyp26b1$^{-/-}$ lungs, the epithelium undergoes relatively normal cell rounding; however, the transition to flattened epithelium is delayed (Fig. 4B,D,F). Although distal epithelial lumens in the mutant lungs can be observed at E16.5, these lumens are appreciably narrower and are open primarily in regions adjacent to the proximal epithelium (Fig. 4G,H, magenta dotted outlines).

As morphological defects arise in Cyp26b1$^{-/-}$ lungs as early as E16.5, we aimed to confirm our previous observation that the total epithelial volume was unchanged at E18.5. We performed flow cytometry on E16.5-E18.5 lungs with the epithelial marker EpCam, which indicated that the total number of epithelial cells did not differ between Cyp26b1$^{+/+}$ and Cyp26b1$^{-/-}$ lungs at any of the three time points examined (Fig. 4I). We next sought to determine whether proliferation rates were increased at earlier stages of lung development at a time when Cyp26b1 mutant lungs begin to display an increase in cellular density. Phospho-Histone H3 (pHH3) staining for proliferating cells revealed a small but significant increase in proliferation only at E18.5, indicating that altered proliferation alone cannot account for the observed changes in cellular density seen as early as E16.5 (Fig. 4J).

Recent data have led to the development of new models concerning the origin of mature distal epithelial cells. These data indicate that specification of distal epithelial progenitors to either AT1 or AT2 cells begins as early as E13.5, with AT1 cells arising primarily from HOPX^{+} cells in the stalk region, whereas AT2 cells derive primarily from proSP-C^{+}/Sox9^{+} cells at the most distal tips (Frank et al., 2019; Jain et al., 2015). Based on these studies, we sought to determine whether the skewing of AT1 and AT2

Development (2020) 147, dev181560. doi:10.1242/dev.181560

differentiation at E18.5 could be accounted for by changes in early progenitor specification. Staining for HOPX (AT1 progenitors) and proSP-C (AT2 progenitors) at E16.5 revealed no overt qualitative differences in AT1 or AT2 progenitor patterning (Fig. 4K,L, magenta dotted outlines). This suggests the observed skewing of AT1 and AT2 cell populations at E18.5 is the result of defects in differentiation and not progenitor specification.

Cyp26b1 mutant lungs exhibit a partial RA transcriptional response

Cyp26b1 is known to dampen RA signaling by catabolizing RA into an inactive metabolite; therefore, we assessed levels of RA signaling in lungs lacking Cyp26b1. As RA primarily effects cellular change by modulating gene transcription, we assayed for genes involved in RA metabolism by qRT-PCR, several of which are direct targets of RA signaling (*Rarb*, *Stra6*, *Crabp2*, *Rbp1*) (Balmer and Blomhoff, 2002; Rhinn and Dolle, 2012; Ross and Zolfaghari, 2011; Wu and Ross, 2010). Transcriptional analyses of these genes in E18.5 whole-lung lysates revealed significant upregulation of *Rarb* and *Stra6*, significant downregulation of the RA-synthesizing enzymes *Raldh1* and *Raldh3*, and a trend towards increased and decreased expression of *Crabp2* and *Raldh2*, respectively (Fig. 5A). We validated these results by performing ISH for *Raldh1*. We found that *Raldh1* is expressed specifically in the proximal epithelium, consistent with previous data, and that loss of Cyp26b1 led to a decrease in its expression in those cells (Fig. S8A,B) (Chazaud et al., 2003).

As Cyp26 family genes can also be regulated by RA (Rhinn and Dolle, 2012; Ross and Zolfaghari, 2011; Wu and Ross, 2010), we investigated their expression in Cyp26b1$^{-/-}$ lungs. We first verified the gene deletion by assessing *Cyp26b1* expression using primers within the deleted region (Fig. 5B, Cyp26b1-E4-5). Repeating the qRT-PCR using primers outside of the deleted region demonstrated that remaining *Cyp26b1* transcript is strongly upregulated in Cyp26b1$^{-/-}$ lungs (Fig. 5B, Cyp26b1). Interestingly, expression levels of *Cyp26a1* and *Cyp26c1* were unaffected (Fig. 5B). ISH and FISH for *Cyp26b1* in mutant lungs co-stained with Emcn validated the qRT-PCR data and revealed that the upregulation of *Cyp26b1* came specifically from ECs (Fig. 5C-H).

We next asked whether other targets of RA signaling are altered in Cyp26b1$^{-/-}$ lungs. We first analyzed expression levels of *Ret*,

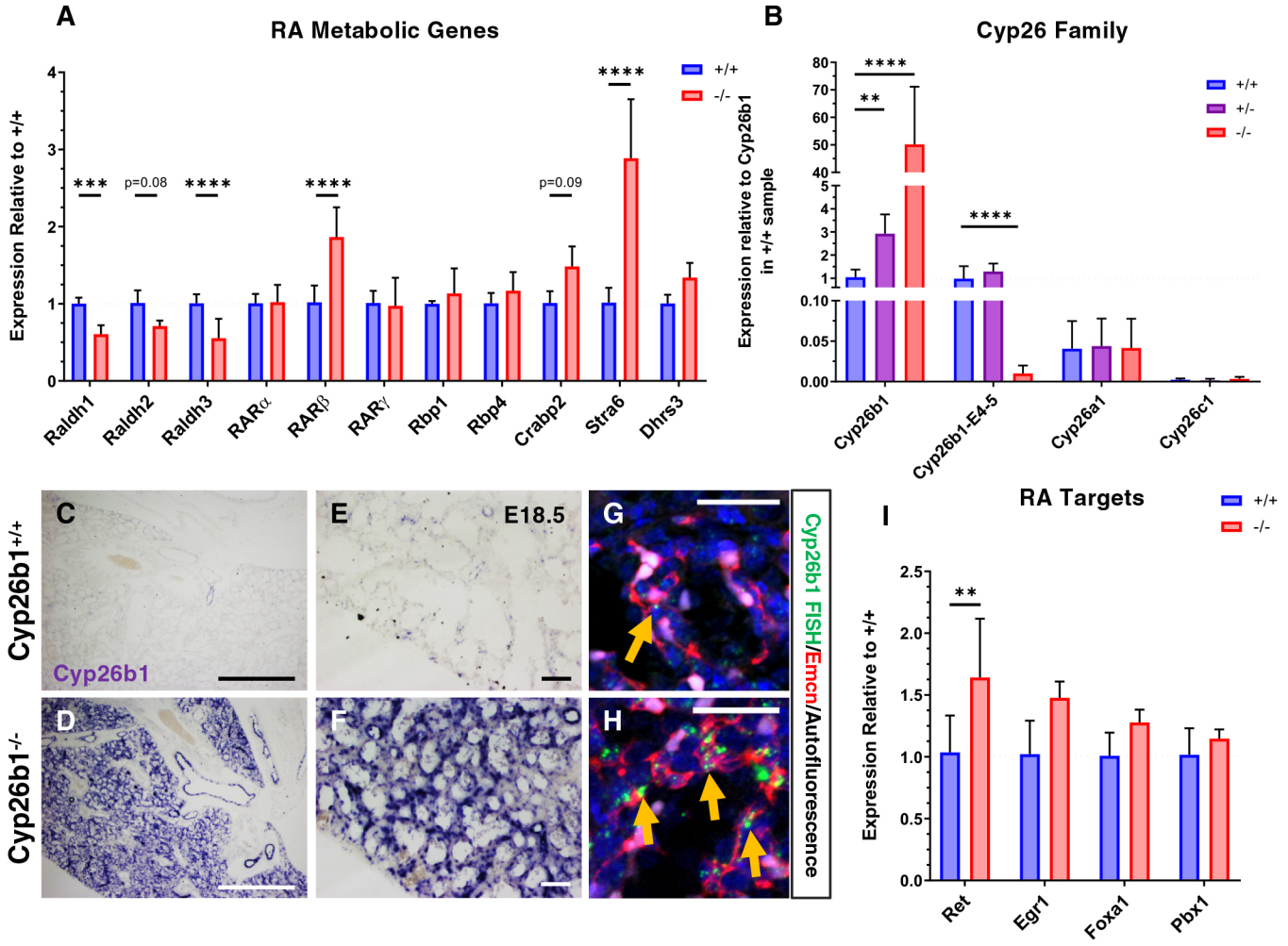

Fig. 5. Cyp26b1$^{-/-}$ lungs exhibit a mixed RA response. (A) qRT-PCR for several RA metabolic genes in whole E18.5 lungs standardized to the expression of +/+ samples for each gene. *n*=6. (B) qRT-PCR for the three Cyp26 family members all standardized to the expression of Cyp26b1 in Cyp26b1$^{+/+}$ samples. 'Cyp26b1' uses primers outside of the deleted region in the Cyp26b1^{-} line, whereas 'Cyp26b1-E4-5' uses primers designed within the deleted region. *n*=4. (C-F) ISH for Cyp26b1 in E18.5 Cyp26b1$^{+/+}$ (C,E) and Cyp26b1$^{-/-}$ (D,F) lungs at 5× (C,D) and 20× (E,F) zoom. (G,H) FISH for Cyp26b1 (green) co-stained with Emcn (red). Orange arrows, Cyp26b1^{+} punctae in ECs. (I) qRT-PCR for *Ret*, *Egr1*, *Foxa1* and *Pbx1* in whole E18.5 lungs. *n*=4. Data are mean±s.d. ***P*<0.01, ****P*<0.001, *****P*<0.0001. Significance was determined using two-way ANOVA with Sidak multiple comparison test on the ΔΔCt values. Scale bars: 500 µm (C,D); 100 µm (E,F); 25 µm (G,H).

Development (2020) 147, dev181560. doi:10.1242/dev.181560

Egr1, *Foxa1* and *Pbx1*, which have all been shown to be direct targets of RA signaling in other contexts (Balmer and Blomhoff, 2002; Probst et al., 2011; Rhinn and Dolle, 2012; Wong et al., 2012). qRT-PCR analyses of whole-lung lysates for these genes revealed significant upregulation of *Ret* alone (Fig. 5I). We similarly asked whether other genes in other signaling pathways may also be differentially regulated. During early lung morphogenesis, RA regulates multiple signaling pathways, including Fgfs, Tgf-β/Bmps, Wnts and Shh (Chen et al., 2007; Desai et al., 2004; Malpel et al., 2000; Rankin et al., 2016, 2018). Surprisingly, qRT-PCR analysis for all of these pathways showed no change, except for downregulation of the Tgf-β target *Tgfbi* (Fig. S8C-F). Taken together, these data indicate that loss of Cyp26b1 can lead to a partial RA response in the lung, in which genes involved in RA metabolism are transcriptionally altered but other established downstream targets are unaffected.

RA partially contributes to the Cyp26b1$^{-/-}$ phenotype in the lung

We sought to more clearly determine whether increased RA is sufficient to induce the changes seen in the Cyp26b1$^{-/-}$ lungs. Previous reports have shown that exogenous administration of atRA can partially phenocopy the defects in limb development, palate fusion and skin barrier formation that are seen in Cyp26b1$^{-/-}$ embryos (Cadot et al., 2012; Okano et al., 2012b). Following a similar dosing regimen, we gavaged atRA to Cyp26b1$^{+/-}$ pregnant dams at E15.5, E16.5 and E17.5, dissected out the lungs at E18.5, and assessed for changes in lung development (Fig. 6A). Of embryos receiving exogenous atRA, 100% of Cyp26b1$^{-/-}$ and ∼30% of Cyp26b1$^{+/-}$ and Cyp26b1$^{+/+}$ died *in utero*, and the remainder died shortly after birth (Fig. 6B). As all atRA-treated Cyp26b1$^{-/-}$ embryos were dead by E18.5, we focused our analysis on the lungs of atRA-treated Cyp26b1$^{+/+}$ and Cyp26b1$^{+/-}$ embryos. atRA-treated Cyp26b1$^{+/+}$ and Cyp26b1$^{+/-}$ lungs exhibited a loss of distal airspaces and increased cellular density that were indistinguishable from control Cyp26b1$^{-/-}$ lungs (Fig. 6C-L,W, Fig. S9A-E). Sox9^{+} distal tip progenitor cells were relatively more abundant in atRA-treated lungs per given area compared with their matched controls, but not to the same degree as in Cyp26b1$^{-/-}$ lungs (Fig. 6M-Q,X). Interestingly, proSP-C^{+} AT2 cells were only proportionally increased in atRA-treated Cyp26b1$^{+/-}$ lungs, but not in atRA-treated Cyp26b1$^{+/+}$ lungs (Fig. 6R-V,Y). These data show that excess RA is sufficient to induce morphologic changes in Cyp26b1$^{-/-}$ lungs but does not fully recapitulate loss of Cyp26b1.

Exogenous RA and loss of Cyp26b1 exhibit distinct transcriptional responses

To further validate these data, we performed qRT-PCR to assess whether RA treatment induces the same changes in transcription as loss of Cyp26b1 in the lung. Consistent with previous results, exogenous atRA treatment induced expression of *Rarb*, *Stra6* and *Cyp26b1* (Fig. S9F,G). We also observed a small, but significant, increase in *Cyp26a1* (Fig. S9G). Next, we assayed for changes in markers of each distal epithelial population. Although expression levels of *Sftpc*, *Aqp5*, *Pdpn*, *Ager* and *HOPX* in atRA-treated lungs mirrored that of Cyp26b1$^{-/-}$ lungs, *Sox9* expression was increased and *CCSP* expression was decreased in atRA-treated lungs only (Fig. 6Z, Fig. S9H). These data raise the possibility that exogenous RA may induce additional transcriptional changes not observed in Cyp26b1$^{-/-}$ lungs, suggesting that Cyp26b1 may play novel roles beyond reduction of RA levels. Indeed, qRT-PCR analysis of potential signaling pathways downstream of RA reveal differential expression of several Shh, Wnt and Tgf-β members in atRA-treated lungs that are not differentially expressed in control Cyp26b1$^{-/-}$ lungs (Fig. 7A-D). Specifically, we found upregulation of *Gli2*, *Gli3*, *Wnt4*, *Tgfb2* and *Tgfb3* in atRA-treated lungs compared with Cyp26b1$^{-/-}$ lungs. In addition, several other genes – namely *Wnt2*, *Tgfbr2*, *Tgfbr3*, *Id1*, *Shh* and *Ptch1* – were not differentially expressed between atRA-treated and Cyp26b1$^{-/-}$ lungs but showed significant differences when the atRA-treated lungs were compared with their genotyped-matched controls (Fig. 7). These data show that exogenous administration of atRA and loss of Cyp26b1 both lead to similar morphogenetic effects on lung development, but do so via partially overlapping but distinct transcriptional mechanisms.

DISCUSSION

Here, we identify a novel role for Cyp26b1 in lung development. Cyp26b1 is enriched in lung ECs throughout development and loss of Cyp26b1 leads to profound changes in distal epithelial differentiation and morphogenesis, ultimately resulting in neonatal lethality. Cyp26b1$^{-/-}$ lungs exhibit an expansion of distal tip progenitors by E18.5 marked by both Sox9 and Lamp3/proSP-C at the expense of mature gas-exchanging AT1 cells. Currently, the only known function of Cyp26b1 is as a negative regulator of RA; however, our data indicate RA signaling is only partially increased in Cyp26b1$^{-/-}$ lungs. Likewise, administration of exogenous atRA during late lung formation does not fully phenocopy loss of Cyp26b1. Instead, we make the unexpected observation that Cyp26b1$^{-/-}$ and atRA-treated lungs undergo overlapping, but distinct, cellular and transcriptional responses. Therefore, our study both identifies an essential role for Cyp26b1 during lung development and suggests that Cyp26b1 has important roles in lung development beyond RA regulation.

Cyp26b1 enrichment in lung ECs throughout development raises interesting questions and implicates ECs in driving the Cyp26b1$^{-/-}$ phenotype. ECs have been shown to regulate lung development during branching morphogenesis and alveolarization (Del Moral et al., 2006; Jakkula et al., 2000; Lazarus et al., 2011). In addition, ECs are crucial in directing distal epithelial development in models of adult lung regeneration (Ding et al., 2011; Lee et al., 2014; Rafii et al., 2015). Our data suggest a new role for ECs during normal lung development in which ECs express Cyp26b1 to locally decrease RA signaling and promote proper distal epithelial differentiation. Although EC organization and specification appear to be unaltered in the mutants, we observed strong self-upregulation of *Cyp26b1* specifically in ECs of Cyp26b1$^{-/-}$ lungs. Interestingly, there was no compensatory change in *Cyp26a1* or *Cyp26c1* expression. Both Cyp26b1 and Cyp26a1 are known targets of RA (Rhinn and Dolle, 2012; Ross and Zolfaghari, 2011; Wu and Ross, 2010) but it is unclear why both loss of Cyp26b1 and exogenous atRA strongly upregulate only Cyp26b1 and not Cyp26a1 in the lung. Based on these expression patterns, there may be unidentified EC-specific mechanisms that lead to upregulation of Cyp26b1 over the other Cyp26 enzymes. It must be stated that we cannot rule out possible roles played by other cells that express low levels of Cyp26b1. However, both the enrichment of Cyp26b1 in wild-type ECs and the specific upregulation of Cyp26b1 expression in Cyp26b1 null ECs are highly suggestive of an EC-driven phenotype. We hypothesize that ECs expressing Cyp26b1 act as a local sink for RA, thereby reducing local RA signaling and creating an RA gradient within the developing lung.

Recent models of distal epithelial development have demonstrated that specification of AT1 and AT2 cells occurs as early as E13.5 and can be identified by location along the distal epithelial tree and by gene

Development (2020) 147, dev181560. doi:10.1242/dev.181560

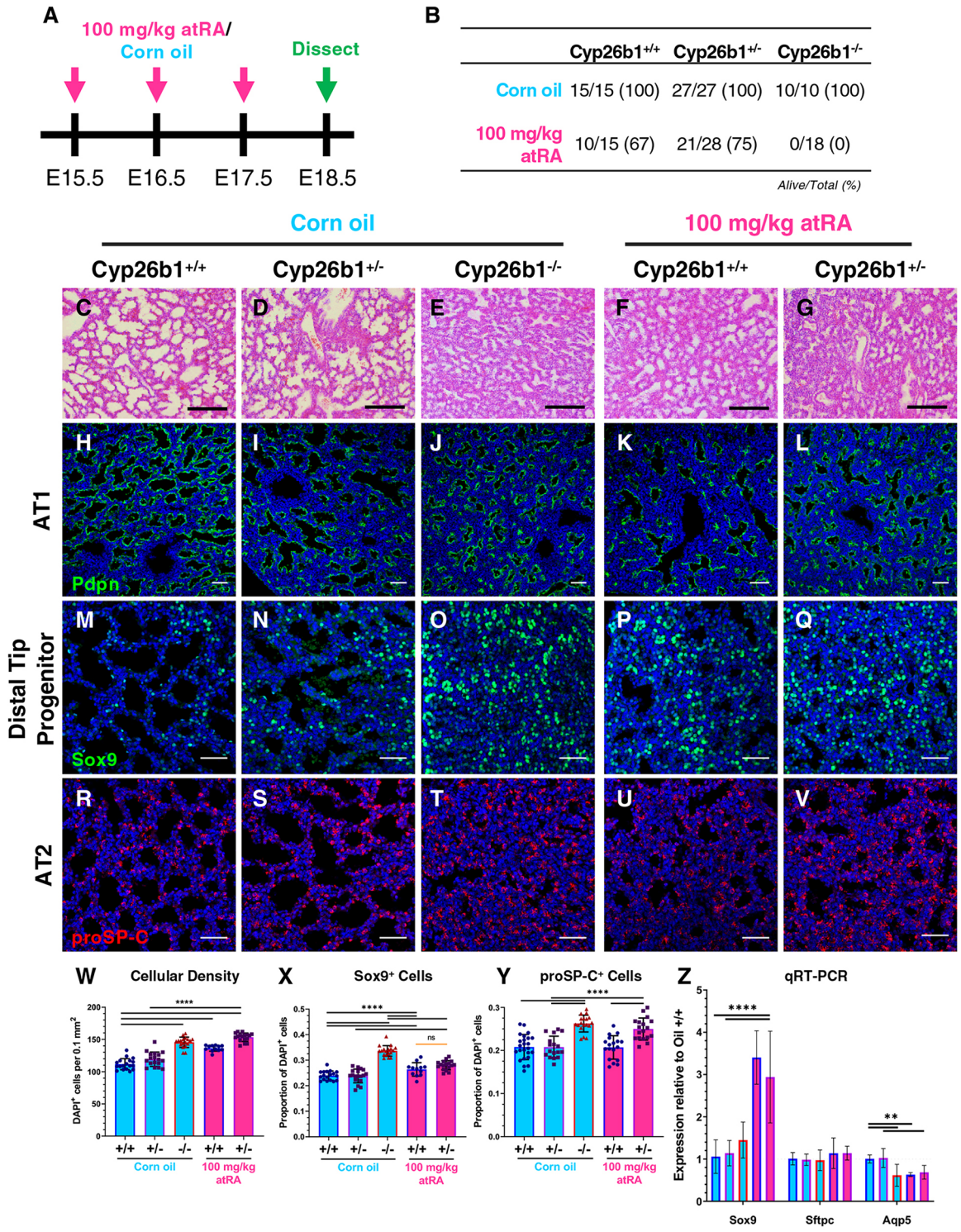

Fig. 6. Exogenous atRA partially phenocopies loss of Cyp26b1. (A) Experimental design for experiments with exogenous atRA: 100 mg/kg atRA (magenta) or equivalent dose of corn oil (control, cyan) was gavaged to pregnant dams at E15.5, E16.5 and E17.5, and dissected at E18.5. (B) Survival chart for E18.5 embryos at the time of dissection for each genotype and treatment. (C-G) H&E stains of control (C-E), and atRA-treated (F-G) lungs at 10× magnification. (H-L) IF stain for the AT1 cell marker Pdpn in control (H-J) and atRA-treated (K-L) lungs. (M-Q) IF stain for Sox9 in control (M-O) and atRA-treated (P-Q) lungs. (R-V) IF stain for the AT2 cell marker proSP-C in control (R-S) and atRA-treated (U-V) lungs. (W) Number of DAPI$^+$ cells per 0.1 mm^2. Outline color corresponds to genotype (blue, Cyp26b1$^{+/+}$; purple, Cyp26b$^{+/-}$; red, Cyp26b1$^{-/-}$) and fill color corresponds to treatment group (cyan, control; magenta; atRA). n=3 with six random views per sample. (X) Quantification of Sox9$^+$ cells in M-Q following the same coloring scheme as in W. n=3 with six random views per sample. (Y) Quantification of proSP-C$^+$ cells in R-V following the same coloring scheme as in W. n=3 with six random views per sample. (Z) qRT-PCR for Sox9, Sftpc and Aqp5 in control and atRA-treated lungs following the same coloring scheme as in W, standardized to the expression of +/+ samples for each gene. n=3 (oil –/–), 4 (oil +/–), 5 (atRA +/–), 6 (oil +/+, atRA +/+). Data are mean±s.d. **P<0.01, ****P<0.0001. Significance was determined using one-way ANOVA with Tukey multiple comparison test (W-Y) and two-way ANOVA with Sidak multiple comparison test on the ΔΔCt values (Z). Scale bars: 500 µm (C-G); 50 µm (H-V).

Development (2020) 147, dev181560. doi:10.1242/dev.181560

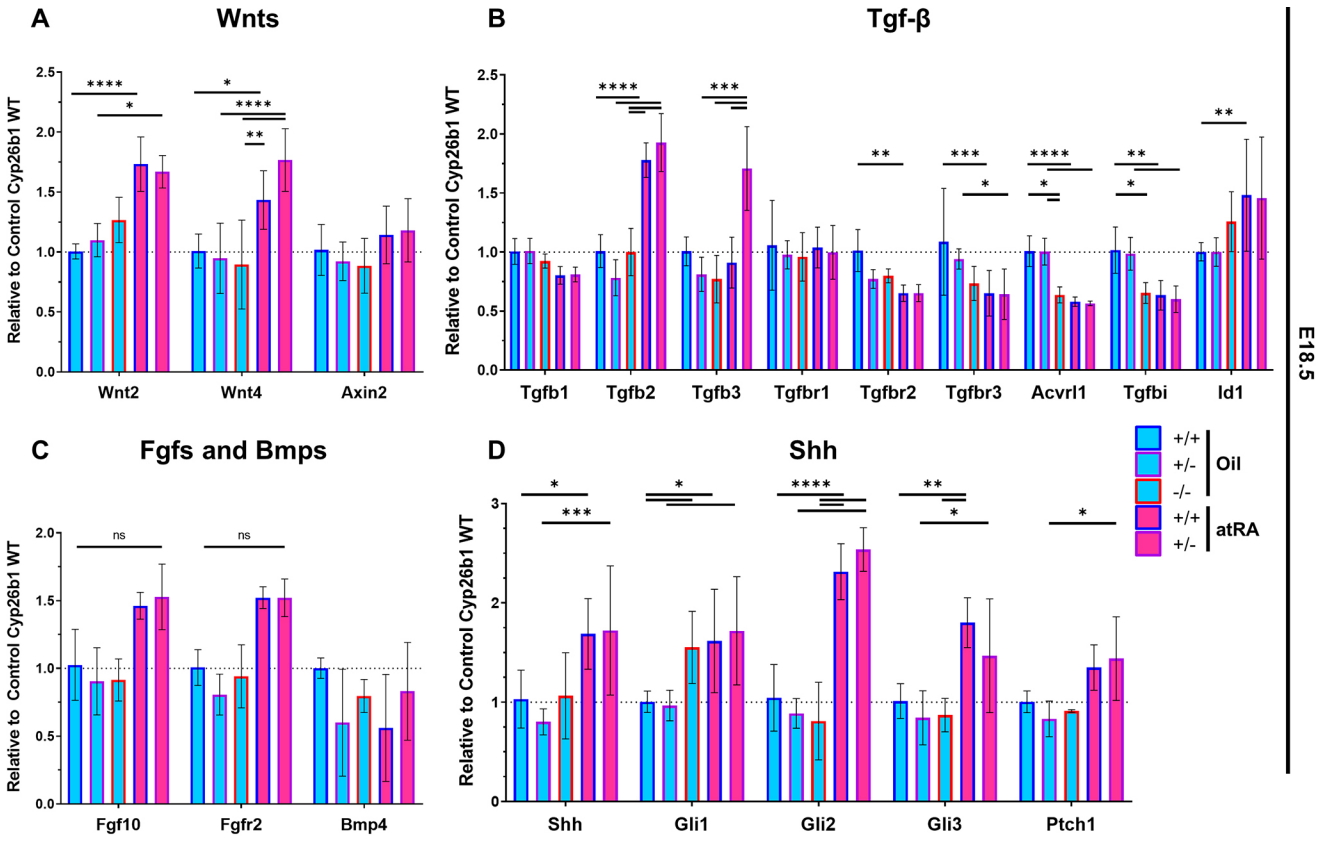

Fig. 7. Exogenous atRA induces distinct transcriptional changes compared with Cyp26b1$^{-/-}$ lungs. (A) qRT-PCR for the Wnt pathway genes *Wnt2*, *Wnt4* and *Axin2* standardized to the expression of +/+ samples for each gene. Outline color corresponds to genotype (blue, Cyp26b1$^{+/+}$; purple, Cyp26b$^{+/-}$; red, Cyp26b1$^{-/-}$) and fill color corresponds to treatment group (cyan, control; magenta, atRA). (B) qRT-PCR for members of the TGF-β signaling pathway following the coloring scheme in A, standardized to the expression of +/+ samples for each gene. (C) qRT-PCR for established regulators of lung branching following the coloring scheme in A, standardized to the expression of +/+ samples for each gene. (D) qRT-PCR for members of the Shh pathway following the coloring scheme in A, standardized to the expression of +/+ samples for each gene. n=3 (oil –/–), 4 (oil +/–), 5 (atRA +/–) and 6 (oil +/+, atRA +/+). Data are mean±s.d. *P<0.05, **P<0.01, ***P<0.001, ****P<0.0001. Significance was determined using two-way ANOVA with Sidak multiple comparison test on the ΔΔCt values. ns, not significant.

expression pattern (Frank et al., 2019). Similarly, our previous work in the pancreas has shown that disruption of early morphogenesis drives shifts in progenitor cell differentiation (Azizoglu et al., 2017). Our analysis here, by contrast, did not reveal overt changes in early patterning of the distal progenitor epithelial tree. Instead, we did observe late defects in cellular morphology, as the transition from columnar to squamous epithelium during terminal differentiation is impaired in the absence of Cyp26b1. This suggests that Cyp26b1 is not required for progenitor specification, but rather it regulates AT1 and AT2 differentiation.

Of note, we observed expansion of distal tip progenitors marked by both Sox9 and Lamp3 at E18.5 possibly at the expense of AT1 cells, whereas the formation of mature Lamp3^{+}/Sox9^{-} AT2 cells was unaffected. Although death in Cyp26b1 mutants was previously characterized as ‘respiratory distress’ (Yashiro et al., 2004), RDS in humans is characterized by decreased surfactant production due to decreased formation of AT2 cells. Instead, we observe an increase in surfactant production upon loss of Cyp26b1. In that regard, our work stands in contrast to other studies that have also identified similar defects in distal epithelial differentiation but found a decrease in surfactant production or proSP-C^{+} AT2 cells (Compernolle et al., 2002; Hogmalm et al., 2014; Kersbergen et al., 2018; Rockich et al., 2013; Woik et al., 2014; Yang et al., 2002). The defects seen in these studies most likely arise from an inability of distal progenitor cells to first differentiate into AT2 cells. By contrast, loss of Cyp26b1 appears to prevent the maturation of AT1, but not AT2, cells which culminates in neonatal lethality.

An important issue arising from our work concerns the role of RA signaling in the phenotype of Cyp26b1 mutants. RA has previously been shown to block distal epithelial differentiation in other contexts. Human pluripotent stem cell-derived lung bud tip organoids containing Sox9^{+} distal progenitors can be maintained in a progenitor state when cultured with Fgf7, CHIR-99021 and RA (Miller et al., 2018). Removal of CHIR-99021 and RA lead to differentiation of these progenitors into the mature airway lineages. Although the effect of removing RA individually was not tested directly, this study is consistent with the model that RA inhibits differentiation of the distal airways. Similarly, hyperactive RA signaling through constitutively active RARα or RARβ leads to defects in distal airway formation (Wongtrakool et al., 2003). Interestingly, lungs with the constitutively active RARα transgene had a complete loss of AT2 and AT1 cells, whereas lungs with the constitutively active RARβ transgene did contain some AT2 and AT1 cells, more closely mirroring Cyp26b1$^{-/-}$ lungs. These data raise the question of the extent to which the effects observed in Cyp26b1$^{-/-}$ lungs are due to elevated RA signaling and whether they are primarily mediated through RARβ or other RARs and nuclear receptors. Whereas these previous studies relied on *in vitro*

Development (2020) 147, dev181560. doi:10.1242/dev.181560

systems or transgenic overexpression systems, we identify Cyp26b1 as an endogenous physiologic mechanism that decreases RA signaling during normal lung development.

To address the role of RA in the Cyp26b1 phenotype, we carried out exogenous administration of atRA beginning at E15.5 and found that it partially phenocopied loss of Cyp26b1. Although morphologic defects in atRA-treated and Cyp26b1$^{-/-}$ lungs were indistinguishable from one another, cell fate changes in atRA-treated lungs did not fully recapitulate that of Cyp26b1$^{-/-}$ lungs. One possible explanation for this is that distal epithelial progenitors are specified as early as E13.5 and may no longer be receptive to RA-driven changes in fate by the first dose of RA at E15.5 (Frank et al., 2019). Cyp26b1$^{-/-}$ lungs are consistently exposed to higher levels of RA throughout lung development, potentially leading to a more severe difference in epithelial differentiation. We confirm the role of RA in driving these morphological defects, as exogenous RA mirrors morphological defects seen upon loss of Cyp26b1. In addition, RA pathway gene expression is similarly altered in RA-treated lungs. However, RA treatment is unable to fully recapitulate cell differentiation defects, but it does lead to additional changes in transcriptional regulation not observed in Cyp26b1$^{-/-}$ lungs, suggesting an additional RA-independent mechanism. First, we saw little change in the expression of multiple signaling pathways known to be regulated by RA during lung development in Cyp26b1$^{-/-}$ lungs. Second, several genes in these pathways were differentially expressed in atRA-treated lungs but not in Cyp26b1$^{-/-}$ lungs. Additional studies need to be performed to identify RA-independent mechanisms driving defects in Cyp26b1$^{-/-}$ lungs.

From our studies, it is clear that Cyp26b1 is essential for the development of a functional lung through its impact on differentiation of distal lung epithelium. As Cyp26b1 is enriched in ECs, we propose that our study identifies Cyp26b1 as a novel endothelial modulator for RA activity in embryonic organs. Given that Cyp26b1 null lungs display increased cellular density and contain an expansion of distal tip progenitors at the expense of mature gas-exchanging AT1 cells, it will be of great interest to see whether its loss causes progenitor differentiation defects in other organs which have not yet been studied. Together, our data provide new perspectives on the complex mechanisms by which RA regulates lung development and suggest novel mechanisms downstream of Cyp26b1. Studies of cell-type specific signaling events such as this one will contribute to better understanding of neonatal lung maturation and to the development therapies for newborns with respiratory disease.

MATERIALS AND METHODS

Mice and embryo handling

Experiments were performed in accordance with protocols approved by the University of Texas Southwestern Medical Center (UTSW) Institutional Animal Care and Use Committee. Cyp26b1 mutant alleles were generated using CRISPR/Cas9 as previously described (Yang et al., 2013). In brief, Cas9 mRNA and *in vitro* transcribed single guide (sg)RNAs were injected directly into C57BL/6J oocytes (Transgenic Core Facility, UTSW). sgRNA sequences used are in Table S1. Mice were crossed to generate a mixed CD1/C57BL/6J background, up to five backcrosses. Deletions were validated and characterized by sequencing (Sanger Sequencing Core, UTSW) using the primers indicated in Table S1. Images of whole embryos and organs were taken using an iPhone XS (Apple) and NeoLumar stereomicroscope (Zeiss) using a DP-70 camera (Olympus), respectively.

RA administration to pregnant dams was performed as previously described (Cadot et al., 2012; Okano et al., 2012b). atRA (Sigma-Aldrich) was reconstituted in corn oil at 50 mg/ml. Pregnant dams were gavaged either 100 mg/kg atRA or equivalent dose of corn oil at E15.5, E16.5 and E17.5.

Measurements of embryo and lung weights

Wet and dry weights for the E18.5 embryo lungs were determined as previously described (Murata et al., 2007). Briefly, lungs were dissected out of embryos, blotted dry and weighed to determine the wet weight. Lungs were then dried overnight at 55°C and weighed again to determine the dry weight. Wet and dry weights were standardized to embryonic weight to determine relative wet and dry weights.

Histologic and IF analysis on sections

E12.5-E18.5 embryos, lungs and kidneys were dissected and fixed in 4% paraformaldehyde/PBS overnight at 4°C and embedded in paraffin as previously described (Azizoglu et al., 2017). For Hematoxylin and Eosin (H&E) stains, sections were deparaffinized in xylene, 100% ethanol and 95% ethanol and washed under running water. Slides were then incubated with Hematoxylin (Gill's Method, Fisher Chemical), destained in acid alcohol (99 ml 70% ethanol+1 ml 12N HCl) and blued in 0.1% sodium bicarbonate. Eosin staining was performed by incubating slides with Eosin Y (Acros Organics). Slides were washed under running water after each staining step. Lastly, slides were dehydrated to 100% ethanol, washed in xylene and mounted using Permount. Images were taken using a Zeiss Axiovert 200 M scope and a DP-70 camera (Olympus).

IF stains were performed as previously described (Daniel et al., 2018). Primary antibody incubations were carried out at 4°C overnight (for antibody information and dilutions, see Table S2). Images were obtained using an A1R Nikon confocal microscope.

Digoxigenin-labeled RNA probes and *in situ* hybridizations

The *Cyp26b1* full coding sequence clone was acquired from Dharmacon (BC059246) and linearized using EcoRI. The Raldh1 full coding sequence clone was acquired from Dharmacon (BC044729) and linearized using KpnI. Probe synthesis was performed as previously described (Daniel et al., 2018). Briefly, probes were synthesized at 37°C for 2-4 h in digoxigenin-synthesis reaction mixture with T3 or T7 RNA polymerase (Roche). After synthesis, DNA was eliminated by adding RQ1 DNase I (Promega) and RNA probes were purified using Micro Bio-spin columns (Bio-Rad).Then 10× hybridization stock was prepared at 10 µg/ml by adding the appropriate volume of pre-hybridization buffer.

In situ hybridizations were performed as previously described (Daniel et al., 2018). E12.5-E18.5 embryos, lungs and kidneys were fixed and embedded in paraffin as described above. Images were taken using a Zeiss Axiovert 200 M scope and a DP-70 camera (Olympus).

For fluorescent *in situ* hybridizations, the protocol is the same as the chromogenic assay up to the 0.2× SSC wash on the second day. After that wash, slides were transferred to 100 mM Tris-HCl (pH 7.5), 150 mM NaCl, 0.1% Tween-20 (TNT) and treated with 0.3% H_2O_2 for 30 min before washing in TNT 3× for 5 min. Slides were then blocked in 1% blocking reagent (Perkin Elmer) for at least 1 h at room temperature. Slides were then incubated with anti-Dig-peroxidase (Roche, 1:500), and either rabbit anti-Lyve1 (1:100) or rat anti-Endomucin (1:200) and rat anti-PECAM (1:200) overnight at 4°C (see Table S2 for full antibody information). After primary antibody incubation, slides were washed in TNT and treated with Fluorescein Amplification Reagent (Perkin Elmer, 1:50 in Plus Amplification Diluent) for 15 min at room temperature. Slides were then washed with TNT and incubated with donkey anti-rabbit 555 (Invitrogen, A-31572) or donkey anti-rat 555 (Abcam, ab150154) for 1 h at room temperature. Lastly, slides were incubated with DAPI, washed in TNT and mounted using Prolong Gold Mounting Medium (Thermo Fisher Scientific). Images were obtained using an A1R Nikon confocal microscope.

RNA isolation and qRT-PCR

E18.5 lungs and kidneys were dissected and placed in RNAse-free Eppendorf tubes (Ambion) in which they were manually dissociated using disposable plastic pestles. RNA extraction was performed using the RNeasy Mini Kit (Qiagen) following the manufacturer's instructions. mRNA concentrations were quantified on a NanoDrop 2000c Spectrophotometer (Thermo Fisher Scientific). RNA was standardized to the sample with the lowest concentration and was reverse transcribed using SuperScript III (Invitrogen) kits following the manufacturer's instructions using oligo-dTs.

Development (2020) 147, dev181560. doi:10.1242/dev.181560

Transcripts were quantified using Power SYBR Green PCR Master Mix (Applied Biosciences) on a QuantStudio 3 Real-Time PCR System (Applied Biosciences). Primers used for qRT-PCR are listed in Table S1. Relative levels of transcripts were determined using the ΔΔCt method by first standardizing mean Ct for a given gene to the housekeeping gene cyclophilin (*Ppib*) in the same sample and then calculating changes between samples. Data and statistical analyses were plotted and performed in GraphPad Prism 8.

Flow cytometry

Primary lung cells were isolated from E16.5-E18.5 lungs as previously described (Kim et al., 2005) using pan CD45-FITC, CD31-APC, Sca1 (Ly-6A)-APC-Cy7 (BD Pharmingen), EpCAM-PECy7 (BioLegend) or CD140a-FITC (Thermo Fisher Scientific), with DAPI (Sigma-Aldrich) staining to eliminate dead cells. Whole E16.5-E18.5 lungs were manually dissociated with a pestle in separate microcentrifuge tubes or with forceps in a sterilized petri dish and then incubated with 2.5 mg/ml Collagenase A (Roche) and 20 µg/ml DNAse 1 (Sigma-Aldrich) for 45 min at 37˚C on a nutator. The reaction was stopped by adding wash media (PBS+0.5% bovine serum albumin (BSA)+2 mM EDTA+1 mM $CaCl_2$) to each reaction. Cells were pelleted and incubated with ACK Lysis buffer for 10 min on ice to lyse red blood cells. Next, cells were washed and filtered through 100 µm and 40 µm cell filters before incubating with the antibodies listed above. Cells were then washed again and resuspended with wash media+DAPI for analysis. Samples were analyzed on an LSR II (BD Biosciences) in the UTSW Flow Cytometry Core Facility.

Western blot

Protein extraction and western blot analyses were performed as previously described (Azizoglu et al., 2017). Briefly, E18.5 lungs were mechanically dissociated with a pestle and homogenized in PBS with 10 µg/ml aprotinin, 10 µg/ml leupeptin and 10 µg/ml pepstatin. Triton X-100 was added to each tube to a final concentration of 1%. Samples were frozen at −80°C overnight, thawed and centrifuged at 10,000 ***g*** for 5 min. Protein samples were quantified using Pierce BSA protein assay (Thermo Fisher Scientific) and standardized in Laemmli's SDS-Sample Buffer (Boston BioProducts). Then 40 µg of total protein from each lung lysate were run on a western blot. Antibodies and concentrations used are listed in Table S2.

Quantification and statistical analysis

Cell counting for $DAPI^+$, $pHH3^+$, $proSP\text{-}C^+$, $Lamp3^+$, $HOPX^+$, $Nkx2.1^+$ and $Sox9^+$ cells was performed using Bitplane Imaris v.9.0.2. Positive cells were first marked using the spots function to generate an initial count, followed by manual editing to ensure proper counts. $Lamp3^+/proSP\text{-}C^+$ cells or $Lamp3^+/Sox9^+$ cells were quantified using the 'colocalize spots' function in the Imaris XT analysis package. Images used in these quantifications encompass at least five random views of distal epithelium from at least three embryos per genotype and treatment condition. Images were captured to avoid all proximal epithelial structures that may improperly skew the results. Airspace area and number were calculated using FIJI. First, a threshold was applied to images of distal airways using the DAPI stain such that the areas occupied by cells were mostly filled. Next, the number and sizes of all blank spaces greater than 100 μm^2 were calculated using the Analyze Particles function. The 100 μm^2 threshold was chosen to eliminate false positive blank spaces that are due to gaps in between adjacent $DAPI^+$ cells and not from actual open airspaces.

Data and statistical analyses were plotted and performed in GraphPad Prism 8 for all experiments described. Significance for cell quantifications, qRT-PCR analysis and flow cytometry was determined using unpaired Student's *t*-test or two-way ANOVA with Sidak multiple comparison test. Significance for embryo and lung weights was determined using one-way ANOVA with Tukey multiple comparison test (as specified in figure legends).

Acknowledgements

We thank members of the ReBuilding a Kidney (RBK) consortium for significant discussion and exchange. We thank Drs Denise Marciano, Thomas Carroll, Michael Buszczak and Michael Dellinger for essential reagents and scientific feedback. We also thank members of the Cleaver lab, including Caitlin Braitsch and Anne Ryan, for discussions and critical reading of the manuscript. We thank David Farrar and the UTSW Flow Cytometry Core for assistance with FACS analysis.

Competing interests

The authors declare no competing or financial interests.

Author contributions

Conceptualization: E.D., O.C.; Methodology: E.D.; Validation: E.D., H.R.B., X.G.; Formal analysis: E.D., H.R.B., M.A.C., O.C.; Investigation: E.D., H.R.B., G.I.S., X.G., Y.H.; Resources: E.D., G.I.S., Y.H.; Data curation: E.D., H.R.B.; Writing - original draft: E.D., O.C.; Writing - review & editing: E.D., H.R.B., G.I.S., Y.H., O.C.; Visualization: E.D., H.R.B., O.C.; Supervision: O.C.; Project administration: O.C.; Funding acquisition: O.C.

Funding

This work was supported by the National Institute of Diabetes and Digestive and Kidney Diseases (DK106743, DK079862 to O.C.); the National Heart, Lung, and Blood Institute (HL113498 to O.C.); a Hamon Center for Regenerative Science and Medicine predoctoral fellowship to E.D.; and a National Science Foundation Graduate Research Fellowship (2019241092 to H.R.B.). Deposited in PMC for release after 12 months.

Supplementary information

Supplementary information available online at
http://dev.biologists.org/lookup/doi/10.1242/dev.181560.supplemental

References

Abu-Abed, S., MacLean, G., Fraulob, V., Chambon, P., Petkovich, M. and Dollé, P. (2002). Differential expression of the retinoic acid-metabolizing enzymes CYP26A1 and CYP26B1 during murine organogenesis. *Mech. Dev.* **110**, 173-177. doi:10.1016/S0925-4773(01)00572-X

Azizoglu, D. B., Braitsch, C., Marciano, D. K. and Cleaver, O. (2017). Afadin and RhoA control pancreatic endocrine mass via lumen morphogenesis. *Genes Dev.* **31**, 2376-2390. doi:10.1101/gad.307637.117

Balmer, J. E. and Blomhoff, R. (2002). Gene expression regulation by retinoic acid. *J. Lipid Res.* **43**, 1773-1808. doi:10.1194/jlr.R100015-JLR200

Bowles, J., Secker, G., Nguyen, C., Kazenwadel, J., Truong, V., Frampton, E., Curtis, C., Skoczylas, R., Davidson, T.-L., Miura, N. et al. (2014). Control of retinoid levels by CYP26B1 is important for lymphatic vascular development in the mouse embryo. *Dev. Biol.* **386**, 25-33. doi:10.1016/j.ydbio.2013.12.008

Braitsch, C. M., Combs, M. D., Quaggin, S. E. and Yutzey, K. E. (2012). Pod1/Tcf21 is regulated by retinoic acid signaling and inhibits differentiation of epicardium-derived cells into smooth muscle in the developing heart. *Dev. Biol.* **368**, 345-357. doi:10.1016/j.ydbio.2012.06.002

Cadot, S., Frenz, D. and Maconochie, M. (2012). A novel method for retinoic acid administration reveals differential and dose-dependent downregulation of Fgf3 in the developing inner ear and anterior CNS. *Dev. Dyn.* **241**, 741-758. doi:10.1002/dvdy.23748

Chazaud, C., Dollé, P., Rossant, J. and Mollard, R. (2003). Retinoic acid signaling regulates murine bronchial tubule formation. *Mech. Dev.* **120**, 691-700. doi:10.1016/S0925-4773(03)00048-0

Chen, F., Desai, T. J., Qian, J., Niederreither, K., Lu, J. and Cardoso, W. V. (2007). Inhibition of Tgf beta signaling by endogenous retinoic acid is essential for primary lung bud induction. *Development* **134**, 2969-2979. doi:10.1242/dev.006221

Chen, F., Cao, Y., Qian, J., Shao, F., Niederreither, K. and Cardoso, W. V. (2010). A retinoic acid-dependent network in the foregut controls formation of the mouse lung primordium. *J. Clin. Invest.* **120**, 2040-2048. doi:10.1172/JCI40253

Chen, F., Marquez, H., Kim, Y. K., Qian, J., Shao, F., Fine, A., Cruikshank, W. W., Quadro, L. and Cardoso, W. V. (2014). Prenatal retinoid deficiency leads to airway hyperresponsiveness in adult mice. *J. Clin. Invest.* **124**, 801-811. doi:10.1172/JCI70291

Compernolle, V., Brusselmans, K., Acker, T., Hoet, P., Tjwa, M., Beck, H., Plaisance, S., Dor, Y., Keshet, E., Lupu, F. et al. (2002). Loss of HIF-2alpha and inhibition of VEGF impair fetal lung maturation, whereas treatment with VEGF prevents fatal respiratory distress in premature mice. *Nat. Med.* **8**, 702-710. doi:10.1038/nm721

Daniel, E., Azizoglu, D. B., Ryan, A. R., Walji, T. A., Chaney, C. P., Sutton, G. I., Carroll, T. J., Marciano, D. K. and Cleaver, O. (2018). Spatiotemporal heterogeneity and patterning of developing renal blood vessels. *Angiogenesis* **21**, 617-634. doi:10.1007/s10456-018-9612-y

Del Moral, P.-M., Sala, F. G., Tefft, D., Shi, W., Keshet, E., Bellusci, S. and Warburton, D. (2006). VEGF-A signaling through Flk-1 is a critical facilitator of early embryonic lung epithelial to endothelial crosstalk and branching morphogenesis. *Dev. Biol.* **290**, 177-188. doi:10.1016/j.ydbio.2005.11.022

Desai, T. J., Malpel, S., Flentke, G. R., Smith, S. M. and Cardoso, W. V. (2004). Retinoic acid selectively regulates Fgf10 expression and maintains cell identity in the prospective lung field of the developing foregut. *Dev. Biol.* **273**, 402-415. doi:10.1016/j.ydbio.2004.04.039

Ding, B.-S., Nolan, D. J., Guo, P., Babazadeh, A. O., Cao, Z., Rosenwaks, Z., Crystal, R. G., Simons, M., Sato, T. N., Worgall, S. et al. (2011). Endothelial-derived angiocrine signals induce and sustain regenerative lung alveolarization. *Cell* **147**, 539-553. doi:10.1016/j.cell.2011.10.003

Dranse, H. J., Sampaio, A. V., Petkovich, M. and Underhill, T. M. (2011). Genetic deletion of Cyp26b1 negatively impacts limb skeletogenesis by inhibiting chondrogenesis. *J. Cell Sci.* **124**, 2723-2734. doi:10.1242/jcs.084699

Du, Y., Guo, M., Whitsett, J. A. and Xu, Y. (2015). 'LungGENS': a web-based tool for mapping single-cell gene expression in the developing lung. *Thorax* **70**, 1092-1094. doi:10.1136/thoraxjnl-2015-207035

Du, Y., Kitzmiller, J. A., Sridharan, A., Perl, A. K., Bridges, J. P., Misra, R. S., Pryhuber, G. S., Mariani, T. J., Bhattacharya, S., Guo, M. et al. (2017). Lung Gene Expression Analysis (LGEA): an integrative web portal for comprehensive gene expression data analysis in lung development. *Thorax* **72**, 481-484. doi:10.1136/thoraxjnl-2016-209598

Duester, G. (2008). Retinoic acid synthesis and signaling during early organogenesis. *Cell* **134**, 921-931. doi:10.1016/j.cell.2008.09.002

Frank, D. B., Penkala, I. J., Zepp, J. A., Sivakumar, A., Linares-Saldana, R., Zacharias, W. J., Stolz, K. G., Pankin, J., Lu, M., Wang, Q. et al. (2019). Early lineage specification defines alveolar epithelial ontogeny in the murine lung. *Proc. Natl. Acad. Sci. USA* **116**, 4362-4371. doi:10.1073/pnas.1813952116

Gallacher, D. J., Hart, K. and Kotecha, S. (2016). Common respiratory conditions of the newborn. *Breathe (Sheff)* **12**, 30-42. doi:10.1183/20734735.000716

Guo, M., Du, Y., Gokey, J. J., Ray, S., Bell, S. M., Adam, M., Sudha, P., Perl, A. K., Deshmukh, H., Potter, S. S. et al. (2019). Single cell RNA analysis identifies cellular heterogeneity and adaptive responses of the lung at birth. *Nat. Commun.* **10**, 37. doi:10.1038/s41467-018-07770-1

Herriges, M. and Morrisey, E. E. (2014). Lung development: orchestrating the generation and regeneration of a complex organ. *Development* **141**, 502-513. doi:10.1242/dev.098186

Hogmalm, A., Bry, M., Strandvik, B. and Bry, K. (2014). IL-1β expression in the distal lung epithelium disrupts lung morphogenesis and epithelial cell differentiation in fetal mice. *Am. J. Physiol. Lung Cell. Mol. Physiol.* **306**, L23-L34. doi:10.1152/ajplung.00154.2013

Jain, R., Barkauskas, C. E., Takeda, N., Bowie, E. J., Aghajanian, H., Wang, Q., Padmanabhan, A., Manderfield, L. J., Gupta, M., Li, D. et al. (2015). Plasticity of Hopx(+) type I alveolar cells to regenerate type II cells in the lung. *Nat. Commun.* **6**, 6727. doi:10.1038/ncomms7727

Jakkula, M., Le Cras, T. D., Gebb, S., Hirth, K. P., Tuder, R. M., Voelkel, N. F. and Abman, S. H. (2000). Inhibition of angiogenesis decreases alveolarization in the developing rat lung. *Am. J. Physiol. Lung Cell. Mol. Physiol.* **279**, L600-L607. doi:10.1152/ajplung.2000.279.3.L600

Kersbergen, A., Best, S. A., Dworkin, S., Ah-Cann, C., de Vries, M. E., Asselin-Labat, M. L., Ritchie, M. E., Jane, S. M. and Sutherland, K. D. (2018). Lung morphogenesis is orchestrated through Grainyhead-like 2 (Grhl2) transcriptional programs. *Dev. Biol.* **443**, 1-9. doi:10.1016/j.ydbio.2018.09.002

Kim, C. F. B., Jackson, E. L., Woolfenden, A. E., Lawrence, S., Babar, I., Vogel, S., Crowley, D., Bronson, R. T. and Jacks, T. (2005). Identification of bronchioalveolar stem cells in normal lung and lung cancer. *Cell* **121**, 823-835. doi:10.1016/j.cell.2005.03.032

Kraus, M. R. C. and Grapin-Botton, A. (2012). Patterning and shaping the endoderm in vivo and in culture. *Curr. Opin. Genet. Dev.* **22**, 347-353. doi:10.1016/j.gde.2012.05.002

Lazarus, A., Del-Moral, P. M., Ilovich, O., Mishani, E., Warburton, D. and Keshet, E. (2011). A perfusion-independent role of blood vessels in determining branching stereotypy of lung airways. *Development* **138**, 2359-2368. doi:10.1242/dev.060723

Lee, J.-H., Bhang, D. H., Beede, A., Huang, T. L., Stripp, B. R., Bloch, K. D., Wagers, A. J., Tseng, Y.-H., Ryeom, S. and Kim, C. F. (2014). Lung stem cell differentiation in mice directed by endothelial cells via a BMP4-NFATc1-thrombospondin-1 axis. *Cell* **156**, 440-455. doi:10.1016/j.cell.2013.12.039

Lenti, E., Farinello, D., Yokoyama, K. K., Penkov, D., Castagnaro, L., Lavorgna, G., Wuputra, K., Sandell, L. L., Tjaden, N. E. B., Bernassola, F. et al. (2016). Transcription factor TLX1 controls retinoic acid signaling to ensure spleen development. *J. Clin. Invest.* **126**, 2452-2464. doi:10.1172/JCI82956

Lindstrom, N. O., De Sena Brandine, G., Tran, T., Ransick, A., Suh, G., Guo, J., Kim, A. D., Parvez, R. K., Ruffins, S. W., Rutledge, E. A. et al. (2018). Progressive recruitment of mesenchymal progenitors reveals a time-dependent process of cell fate acquisition in mouse and human nephrogenesis. *Dev. Cell* **45**, 651-660.e654. doi:10.1016/j.devcel.2018.05.010

Malpel, S., Mendelsohn, C. and Cardoso, W. V. (2000). Regulation of retinoic acid signaling during lung morphogenesis. *Development* **127**, 3057-3067.

Massaro, G. D. and Massaro, D. (1996). Postnatal treatment with retinoic acid increases the number of pulmonary alveoli in rats. *Am. J. Physiol.* **270**, L305-L310. doi:10.1152/ajplung.1996.270.2.L305

Massaro, G. D. and Massaro, D. (2000). Retinoic acid treatment partially rescues failed septation in rats and in mice. *Am. J. Physiol. Lung Cell. Mol. Physiol.* **278**, L955-L960. doi:10.1152/ajplung.2000.278.5.L955

Massaro, G. D. C., Massaro, D. and Chambon, P. (2003). Retinoic acid receptor-alpha regulates pulmonary alveolus formation in mice after, but not during, perinatal period. *Am. J. Physiol. Lung Cell. Mol. Physiol.* **284**, L431-L433. doi:10.1152/ajplung.00245.2002

McGowan, S., Jackson, S. K., Jenkins-Moore, M., Dai, H.-H., Chambon, P. and Snyder, J. M. (2000). Mice bearing deletions of retinoic acid receptors demonstrate reduced lung elastin and alveolar numbers. *Am. J. Respir. Cell Mol. Biol.* **23**, 162-167. doi:10.1165/ajrcmb.23.2.3904

Metzger, R. J., Klein, O. D., Martin, G. R. and Krasnow, M. A. (2008). The branching programme of mouse lung development. *Nature* **453**, 745-750. doi:10.1038/nature07005

Miller, A. J., Hill, D. R., Nagy, M. S., Aoki, Y., Dye, B. R., Chin, A. M., Huang, S., Zhu, F., White, E. S., Lama, V. et al. (2018). *In Vitro* induction and *In Vivo* engraftment of lung bud tip progenitor cells derived from human pluripotent stem cells. *Stem Cell Reports* **10**, 101-119. doi:10.1016/j.stemcr.2017.11.012

Morrisey, E. E. and Hogan, B. L. M. (2010). Preparing for the first breath: genetic and cellular mechanisms in lung development. *Dev. Cell* **18**, 8-23. doi:10.1016/j.devcel.2009.12.010

Murata, T., Lin, M. I., Huang, Y., Yu, J., Bauer, P. M., Giordano, F. J. and Sessa, W. C. (2007). Reexpression of caveolin-1 in endothelium rescues the vascular, cardiac, and pulmonary defects in global caveolin-1 knockout mice. *J. Exp. Med.* **204**, 2373-2382. doi:10.1084/jem.20062340

Okano, J., Kimura, W., Papaionnou, V. E., Miura, N., Yamada, G., Shiota, K. and Sakai, Y. (2012a). The regulation of endogenous retinoic acid level through CYP26B1 is required for elevation of palatal shelves. *Dev. Dyn.* **241**, 1744-1756. doi:10.1002/dvdy.23862

Okano, J., Lichti, U., Mamiya, S., Aronova, M., Zhang, G., Yuspa, S. H., Hamada, H., Sakai, Y. and Morasso, M. I. (2012b). Increased retinoic acid levels through ablation of Cyp26b1 determine the processes of embryonic skin barrier formation and peridermal development. *J. Cell Sci.* **125**, 1827-1836. doi:10.1242/jcs.101550

Park, W. Y., Miranda, B., Lebeche, D., Hashimoto, G. and Cardoso, W. V. (1998). FGF-10 is a chemotactic factor for distal epithelial buds during lung development. *Dev. Biol.* **201**, 125-134. doi:10.1006/dbio.1998.8994

Probst, S., Kraemer, C., Demougin, P., Sheth, R., Martin, G. R., Shiratori, H., Hamada, H., Iber, D., Zeller, R. and Zuniga, A. (2011). SHH propagates distal limb bud development by enhancing CYP26B1-mediated retinoic acid clearance via AER-FGF signalling. *Development* **138**, 1913-1923. doi:10.1242/dev.063966

Rafii, S., Cao, Z., Lis, R., Siempos, I. I., Chavez, D., Shido, K., Rabbany, S. Y. and Ding, B.-S. (2015). Platelet-derived SDF-1 primes the pulmonary capillary vascular niche to drive lung alveolar regeneration. *Nat. Cell Biol.* **17**, 123-136. doi:10.1038/ncb3096

Rankin, S. A., Han, L., McCracken, K. W., Kenny, A. P., Anglin, C. T., Grigg, E. A., Crawford, C. M., Wells, J. M., Shannon, J. M. and Zorn, A. M. (2016). A retinoic acid-hedgehog cascade coordinates mesoderm-inducing signals and endoderm competence during lung specification. *Cell Rep* **16**, 66-78. doi:10.1016/j.celrep.2016.05.060

Rankin, S. A., McCracken, K. W., Luedeke, D. M., Han, L., Wells, J. M., Shannon, J. M. and Zorn, A. M. (2018). Timing is everything: reiterative Wnt, BMP and RA signaling regulate developmental competence during endoderm organogenesis. *Dev. Biol.* **434**, 121-132. doi:10.1016/j.ydbio.2017.11.018

Rhinn, M. and Dolle, P. (2012). Retinoic acid signalling during development. *Development* **139**, 843-858. doi:10.1242/dev.065938

Rockich, B. E., Hrycaj, S. M., Shih, H. P., Nagy, M. S., Ferguson, M. A. H., Kopp, J. L., Sander, M., Wellik, D. M. and Spence, J. R. (2013). Sox9 plays multiple roles in the lung epithelium during branching morphogenesis. *Proc. Natl. Acad. Sci. USA* **110**, E4456-E4464. doi:10.1073/pnas.1311847110

Ross, A. C. and Zolfaghari, R. (2011). Cytochrome P450s in the regulation of cellular retinoic acid metabolism. *Annu. Rev. Nutr.* **31**, 65-87. doi:10.1146/annurev-nutr-072610-145127

Sabbagh, M. F., Heng, J. S., Luo, C., Castanon, R. G., Nery, J. R., Rattner, A., Goff, L. A., Ecker, J. R. and Nathans, J. (2018). Transcriptional and epigenomic landscapes of CNS and non-CNS vascular endothelial cells. *Elife* **7**, e36187. doi:10.7554/eLife.36187.042

Shi, W., Chen, F. and Cardoso, W. V. (2009). Mechanisms of lung development: contribution to adult lung disease and relevance to chronic obstructive pulmonary disease. *Proc. Am. Thorac. Soc.* **6**, 558-563. doi:10.1513/pats.200905-031RM

Spoorendonk, K. M., Peterson-Maduro, J., Renn, J., Trowe, T., Kranenbarg, S., Winkler, C. and Schulte-Merker, S. (2008). Retinoic acid and Cyp26b1 are critical regulators of osteogenesis in the axial skeleton. *Development* **135**, 3765-3774. doi:10.1242/dev.024034

Tabula Muris, C., Overall coordination, Logistical coordination, Organ collection and processing, Library preparation and sequencing, Computational data analysis, Cell type annotation, Writing group, Supplemental text writing group, Principal investigators. (2018). Single-cell transcriptomics of 20 mouse organs creates a Tabula Muris. *Nature* **562**, 367-372. doi:10.1038/s41586-018-0590-4

Wang, Z., Dollé, P., Cardoso, W. V. and Niederreither, K. (2006). Retinoic acid regulates morphogenesis and patterning of posterior foregut derivatives. *Dev. Biol.* **297**, 433-445. doi:10.1016/j.ydbio.2006.05.019

Wang, S., Huang, W., Castillo, H. A., Kane, M. A., Xavier-Neto, J., Trainor, P. A. and Moise, A. R. (2018). Alterations in retinoic acid signaling affect the development of the mouse coronary vasculature. *Dev. Dyn.* **247**, 976-991. doi:10.1002/dvdy.24639

Warburton, D., El-Hashash, A., Carraro, G., Tiozzo, C., Sala, F., Rogers, O., Langhe, S. D., Kemp, P. J., Riccardi, D., Torday, J. et al. (2010). Lung organogenesis. In *Organogenesis in Development* (ed. P. Koopman), pp. 73-158.

Wilson, J. G., Roth, C. B. and Warkany, J. (1953). An analysis of the syndrome of malformations induced by maternal vitamin A deficiency. Effects of restoration of vitamin A at various times during gestation. *Am. J. Anat.* **92**, 189-217. doi:10.1002/aja.1000920202

Woik, N., Dietz, C. T., Schaker, K. and Kroll, J. (2014). Kelch-like ECT2-interacting protein KLEIP regulates late-stage pulmonary maturation via Hif-2alpha in mice. *Dis. Model Mech.* **7**, 683-692. doi:10.1242/dmm.014266

Wong, Y. F., Wilson, P. D., Unwin, R. J., Norman, J. T., Arno, M., Hendry, B. M. and Xu, Q. (2012). Retinoic acid receptor-dependent, cell-autonomous, endogenous retinoic acid signaling and its target genes in mouse collecting duct cells. *PLoS ONE* **7**, e45725. doi:10.1371/journal.pone.0045725

Wongtrakool, C., Malpel, S., Gorenstein, J., Sedita, J., Ramirez, M. I., Underhill, T. M. and Cardoso, W. V. (2003). Down-regulation of retinoic acid receptor alpha signaling is required for sacculation and type I cell formation in the developing lung. *J. Biol. Chem.* **278**, 46911-46918. doi:10.1074/jbc.M307977200

Wu, L. and Ross, A. C. (2010). Acidic retinoids synergize with vitamin A to enhance retinol uptake and STRA6, LRAT, and CYP26B1 expression in neonatal lung. *J. Lipid Res.* **51**, 378-387. doi:10.1194/jlr.M001222

Xiao, Y., Hill, M. C., Zhang, M., Martin, T. J., Morikawa, Y., Wang, S., Moise, A. R., Wythe, J. D. and Martin, J. F. (2018). Hippo signaling plays an essential role in cell state transitions during cardiac fibroblast development. *Dev. Cell* **45**, 153-169.e156. doi:10.1016/j.devcel.2018.03.019

Yang, H., Lu, M. M., Zhang, L., Whitsett, J. A. and Morrisey, E. E. (2002). GATA6 regulates differentiation of distal lung epithelium. *Development* **129**, 2233-2246. doi:10.1242/dev.00150

Yang, H., Wang, H., Shivalila, C. S., Cheng, A. W., Shi, L. and Jaenisch, R. (2013). One-step generation of mice carrying reporter and conditional alleles by CRISPR/Cas-mediated genome engineering. *Cell* **154**, 1370-1379. doi:10.1016/j.cell.2013.08.022

Yashiro, K., Zhao, X., Uehara, M., Yamashita, K., Nishijima, M., Nishino, J., Saijoh, Y., Sakai, Y. and Hamada, H. (2004). Regulation of retinoic acid distribution is required for proximodistal patterning and outgrowth of the developing mouse limb. *Dev. Cell* **6**, 411-422. doi:10.1016/S1534-5807(04)00062-0

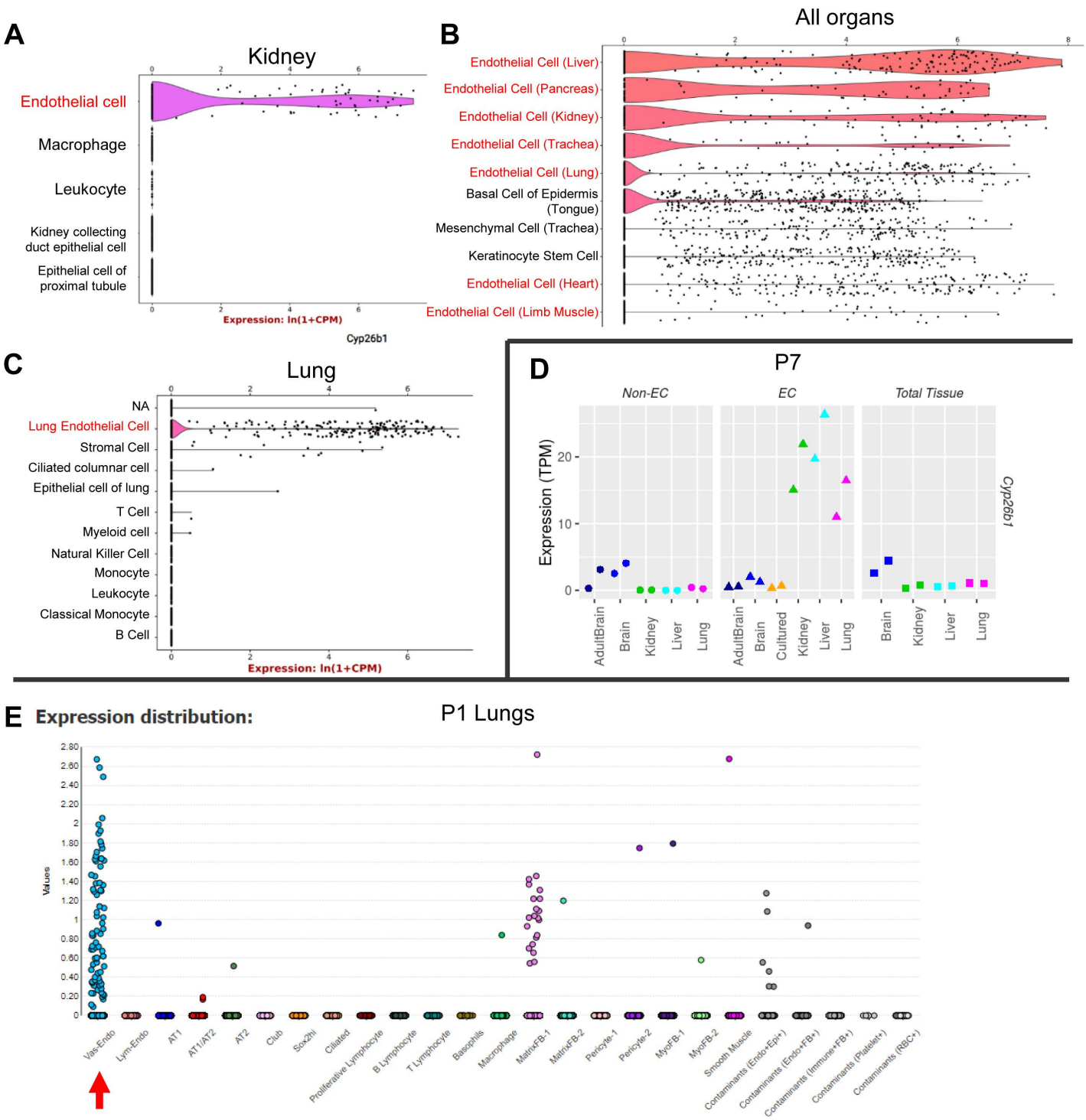

Figure S1. Cyp26b1 is highly enriched in lung, kidney, and other endothelial cell beds in post-natal mice. A-C) Violin plots of Cyp26b1 expression in scRNA-seq of adult kidneys (A), lungs (C), and in all adult organs combined (B) obtained from Tabula Muris consortium (Tabula Muris et al., 2018). EC populations are highlighted in red. Data accessed through https://tabula-muris.ds.czbiohub.org/ D) Bulk RNA-seq of Tie2-GFP^{+} P7 ECs from brain, liver, lung, and kidney compared to GFP^{-} cells (Sabbagh et al., 2018). Data accessed through https://markfsabbagh.shinyapps.io/vectrdb/. E) Scatter plot of Drop-seq analysis of P1 lungs from LungGENS (Du et al., 2015; Du et al., 2017; Guo et al., 2019). Vascular-ECs are marked with Red arrow. Data accessed through https://research.cchmc.org/pbge/lunggens/SCLAB.html.

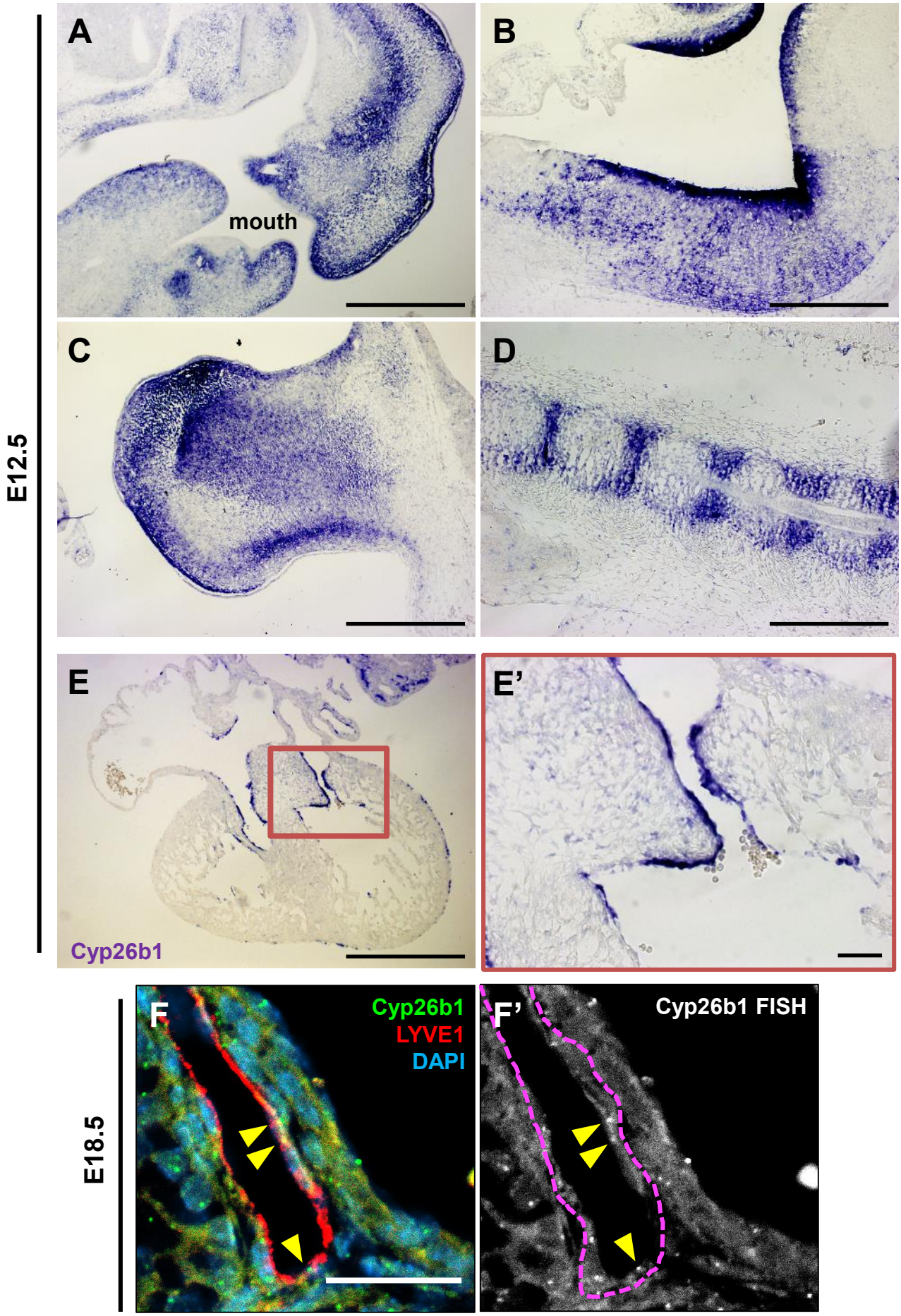

Figure S2. Cyp26b1 is expressed in multiple organs at E12.5. A-E') ISH for Cyp26b1 in the head (A), hindbrain (B), forelimb (C), somites (D), and heart (E). Mouth in (A) is marked for orientation. E') Zoomed in image of endocardial cushion shown in E. F-F') FISH for Cyp26b1 (Green) co-stained with Lyve1 (red). Yellow arrowheads = Cyp26b1 punctae in lymphatic ECs. Lymphatic ECs outlined in magenta (H). Scale bar: 500 μm (A-E); 100 μm (E'); 25 μm (F).

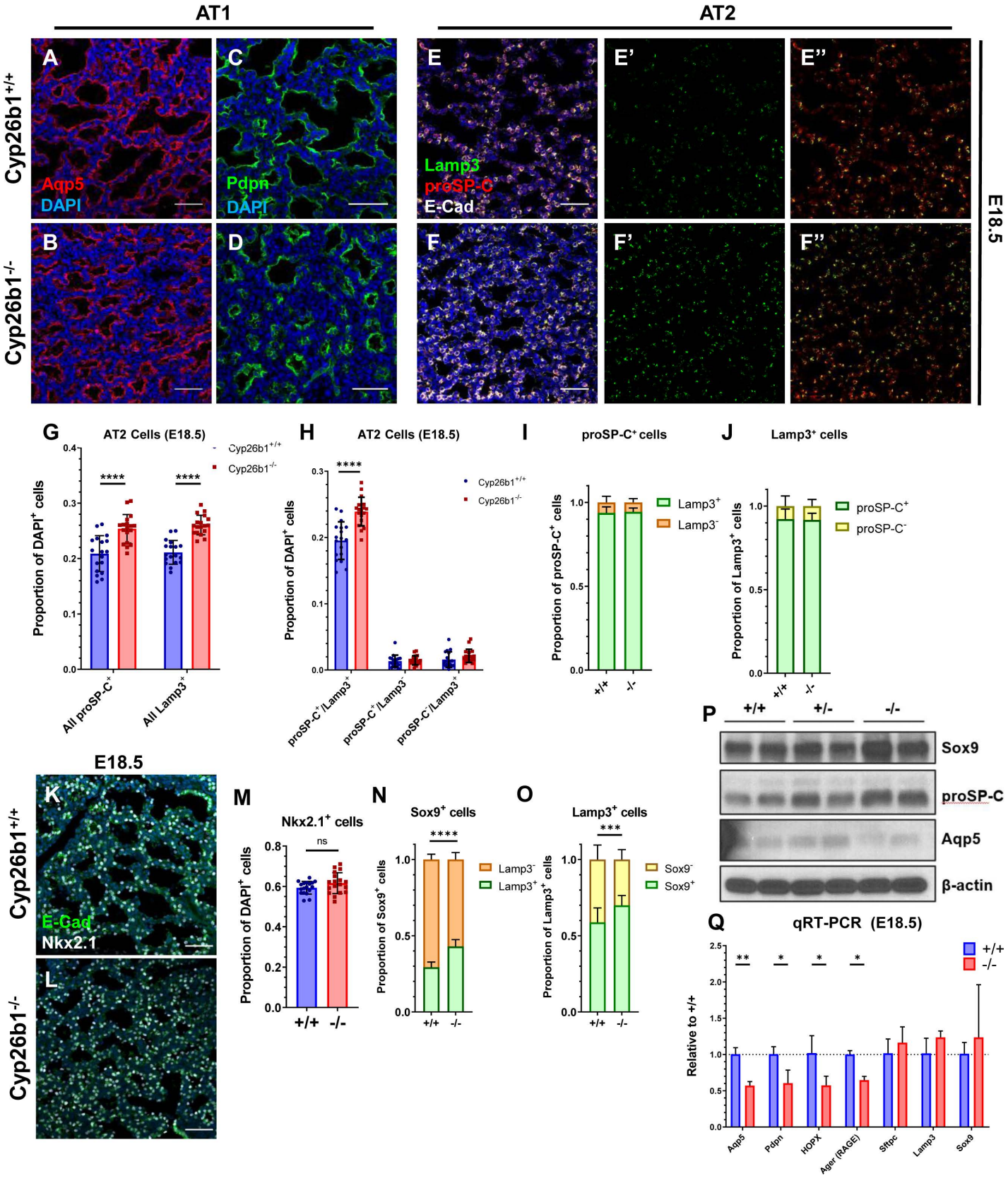

Figure S3. Validation of defects in distal epithelial differentiation using independent AT1 and AT2 cell markers. A-D) IF stain on E18.5 lung for AT1 markers Aqp5 (A-B) and Pdpn (C-D). E-F") IF stain for the AT2 markers Lamp3 and proSP-C. Scale bar = 50 μm. G) Quantification of all proSP-C$^+$ cells and all Lamp3$^+$ cells with respect to DAPI. Bars represent mean ±SD, n=3 biological replicates with 6 random views per sample. Significance determined with two-way ANOVA with Sidak multiple comparison test. ****P<0.0001. H) Stratification of data shown in G into proSP-C/Lamp3 double positive cells (first set), proSP-C single positive cells (second set), and Lamp3 single positive cells (third set) as a proportion of DAPI$^+$ cells. Bars represent mean ±SD. Significance determined with two-way ANOVA with Sidak multiple comparison test. ****P<0.0001. I) Quantification of proSP-C/Lamp3 double positive cells (green) and proSP-C single positive cells (orange) with respect to all proSP-C$^+$ cells. Bars represent mean ±SD, n=3 biological replicates with 6 random views per sample. J) Quantification of proSP-C/Lamp3 double positive cells (green) and Lamp3 single positive cells (yellow) with respect to all Lamp3$^+$ cells. Bars represent mean ±SD, n=3 biological replicates with 6 random views per sample. K-L) IF stain for the epithelial markers Nkx2.1 and E-cad on E18.5 lung. Scale bar = 50 μm. M) Quantification of all Nkx2.1$^+$ with respect to DAPI. Bars represent mean ±SD, n=3 biological replicates with 6 random views per sample. Significance determined with two-way ANOVA with Sidak multiple comparison test. N) Quantification of Lamp3/Sox9 double positive cells (green) and Sox9 single positive cells (orange) with respect to all Sox9$^\pm$ cells. Bars represent mean ±SD, n=3 biological replicates with 5 random views per sample. O) Quantification of Lamp3/Sox9 double positive cells (green) and Lamp3 single positive cells (yellow) with respect to all Lamp3$^\pm$ cells. Bars represent mean ±SD, n=3 biological replicates with 5 random views per sample. P) Western blot analysis of Sox9, proSP-C, and Aqp5 in E18.5 lungs with β-actin as loading control. Q) qRT-PCR analysis for AT1 markers *Aqp5*, *Pdpn*, *HOPX*, and *Ager*, the AT2 markers *Lamp3* and *Sftpc*, and the progenitor marker *Sox9*. Bars represent mean ±SD, n=3 (*Aqp5, HOPX, Ager, Lamp3*), 6 (*Pdpn, Sftpc, Sox9*). Significance was determined using two-way ANOVA with Sidak multiple comparison test on the ΔΔCt values. Significance was determined using two-way ANOVA with Sidak multiple comparison test. *P<0.05, **P<0.01.

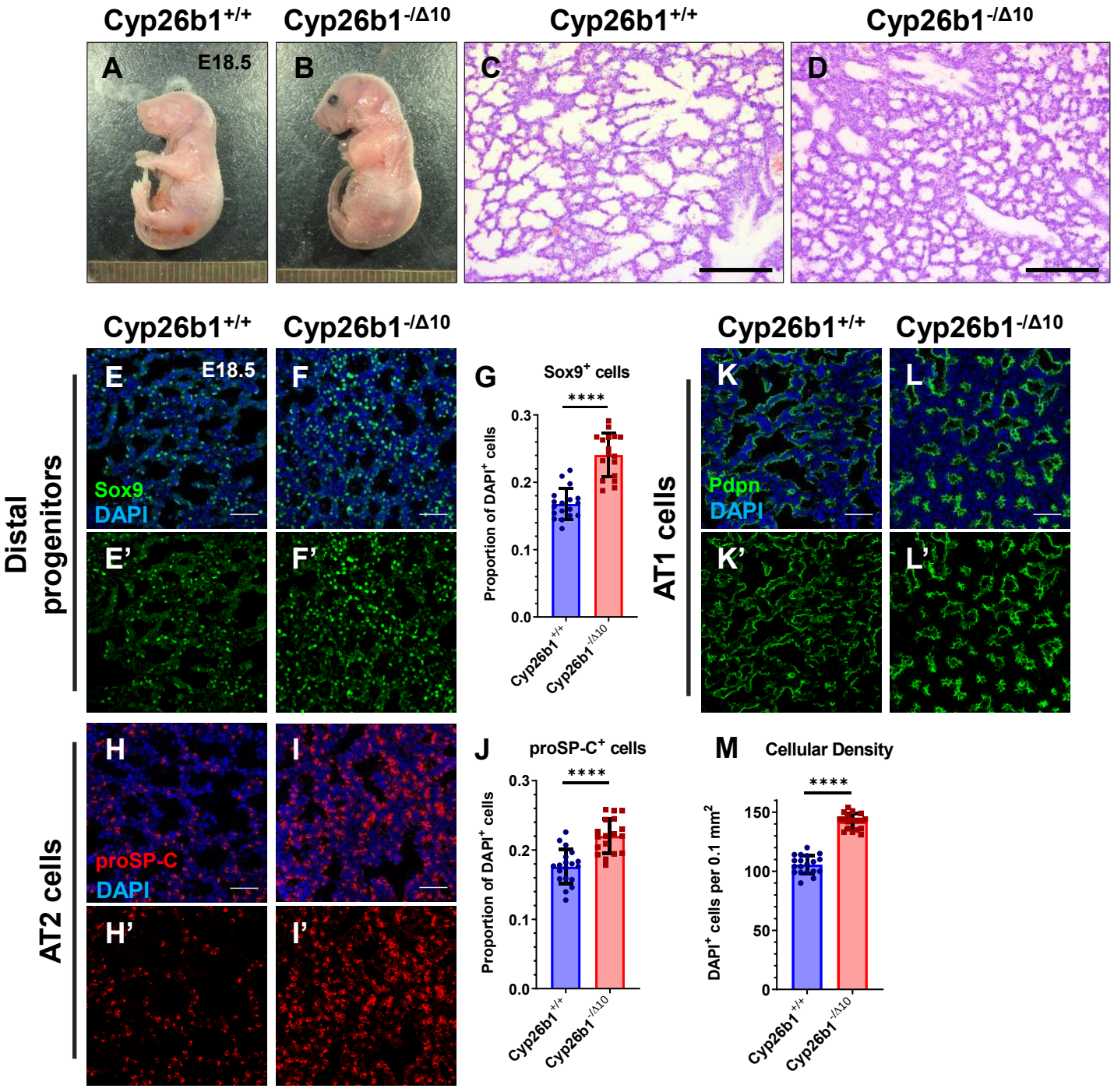

Figure S4. Cyp26b1$^{-/\Delta 10}$ lungs phenocopy Cyp26b1$^{-/-}$ lung defects in increased cellular density and distal epithelial differentiation. A-B) E18.5 Cyp26b1$^{+/+}$ and Cyp26b1$^{-/\Delta 10}$ embryos at dissection. C-D) H&E stain of E18.5 Cyp26b1$^{+/+}$ and Cyp26b1$^{-/\Delta 10}$ lungs at 10x. E-G) IF stain for the Sox9^{+} distal progenitors (E-F') and quantification relative to DAPI^{+} cells (G). Bars represent mean ±SD, n=3 biological replicates with 6 random views per sample. Significance determined with unpaired Student's T-test. ****P<0.0001. H-J) IF stain for the proSP-C^{+} AT2 cells (H-I') and quantification relative to DAPI^{+} cells (J). Bars represent mean ±SD, n=3 biological replicates with 6 random views per sample. Significance determined with unpaired Student's T-test. ****P<0.0001. K-L') IF stain for the Pdpn^{+} AT1 cells. M) Number of DAPI^{+} cells per 0.1 mm^2. Bars represent mean ±SD, n=3 biological replicates with 6 random views per sample. Significance determined with unpaired Student's T-test. ****P<0.0001. Scale bar: 200 μm (C,D); 50 μm (E-F',H-I',K-L').

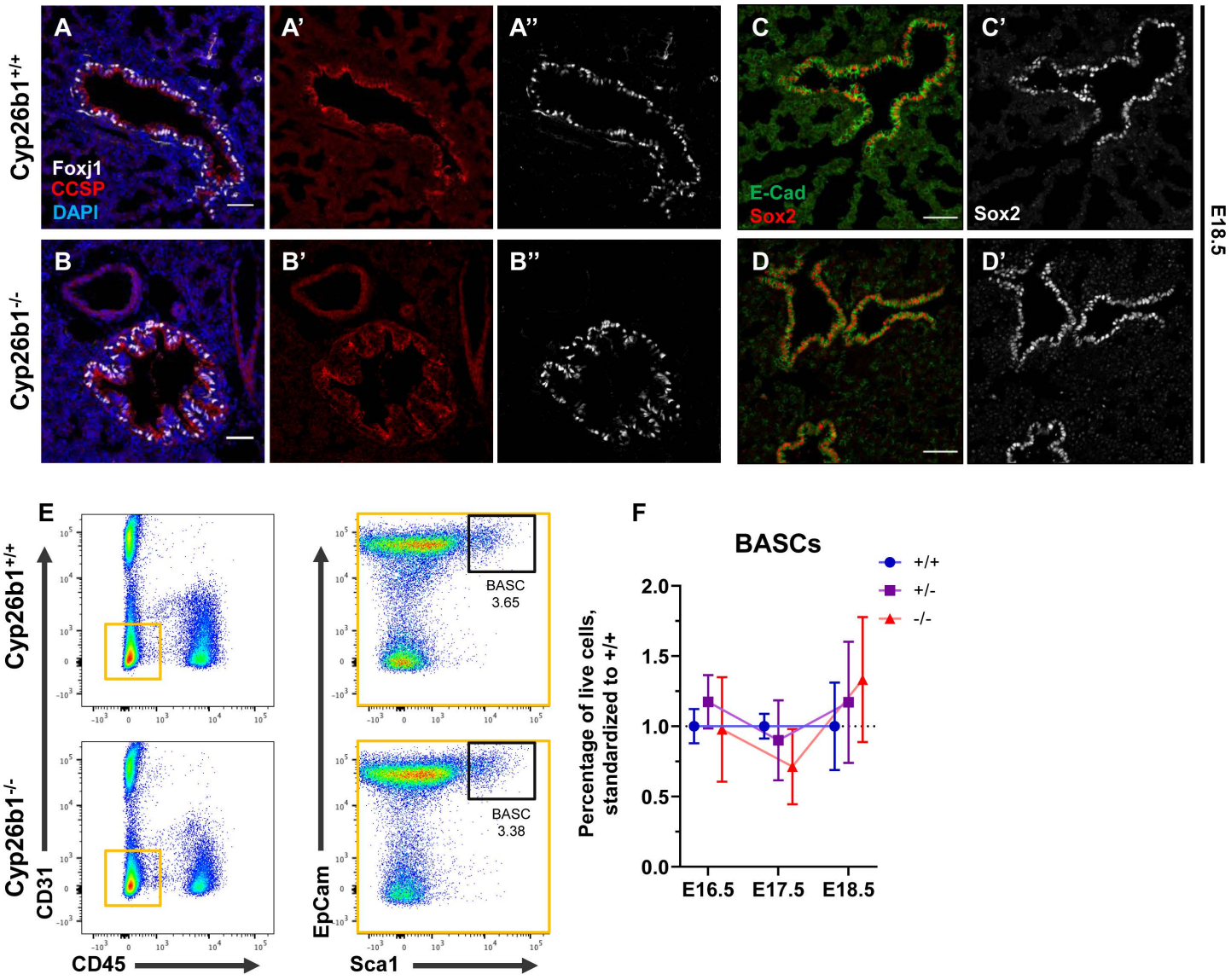

Figure S5. Proximal airways are unaffected in Cyp26b1$^{-/-}$ lungs. A-B") IF stains for CCSP (red) and FoxJ1 (white) in E18.5 Cyp26b1$^{+/+}$ (A-A") and Cyp26b1$^{-/-}$ (B-B") lungs. C-D') IF stains for Sox2 in E18.5 Cyp26b1$^{+/+}$ (C-C') and Cyp26b1$^{-/-}$ (D-D') lungs. Scale bar = 50 μm. E) Representative flow charts for analysis of BASC populations. F) Quantification of the frequency BASCs (CD31^{-}/CD45^{-}/Sca1^{+}/Ep-CAM^{+}) as a proportion of all live cells in E16.5 – E18.5 lungs. Quantifications are standardized to the frequency of BASCs in Cyp26b1$^{+/+}$ samples per experiment. Mean ±SD plotted, n=9 (E16.5 +/+, E17.5 +/+), 4 (E16.5 +/-, E18.5 -/-), 5 (E16.5 -/-, E18.5 +/+), 10 (E17.5 +/-), 6 (E17.5 -/-, E18.6 +/-).

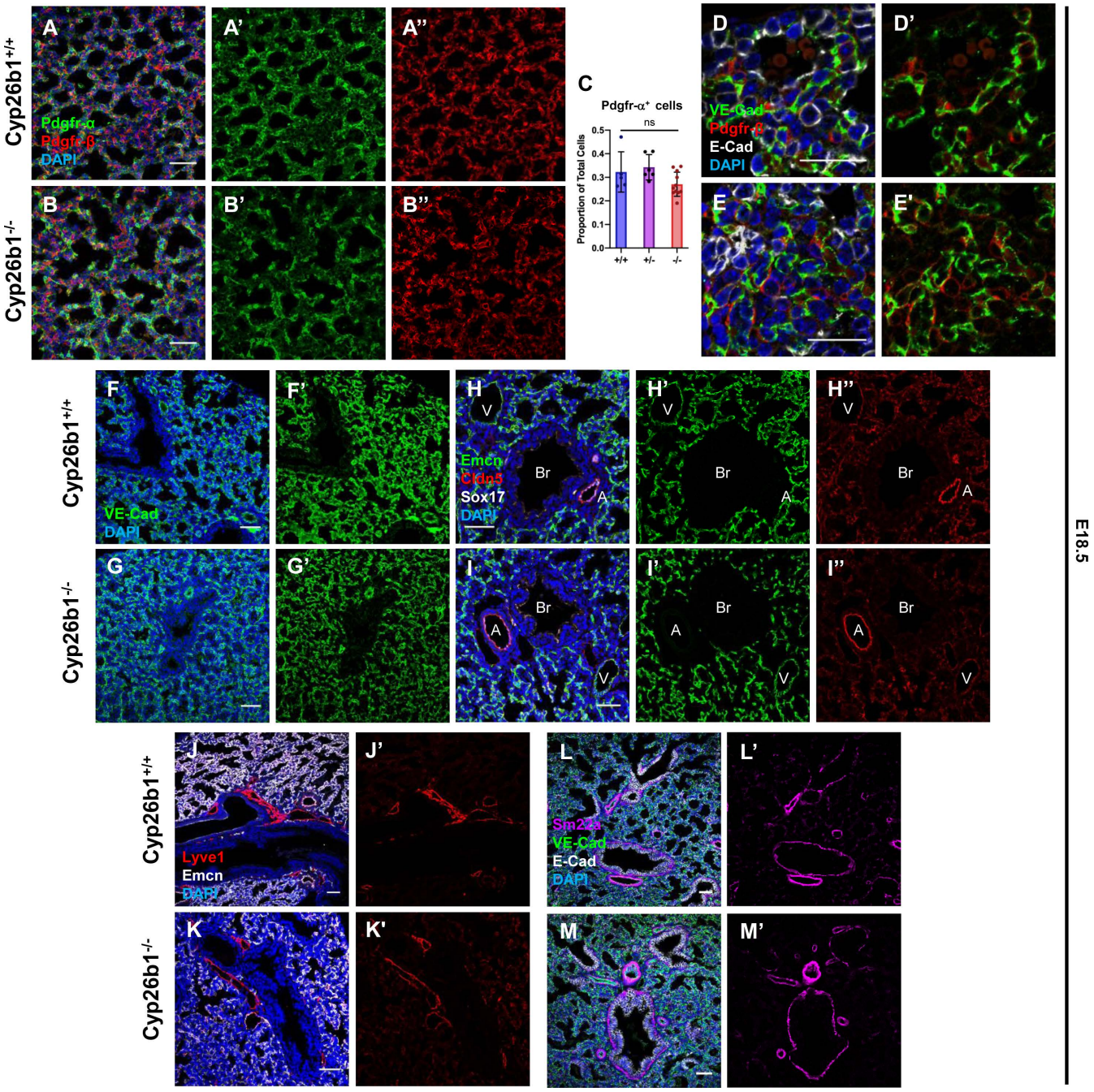

Figure S6. Stromal and vascular lineages are unaffected in Cyp26b1$^{-/-}$ lungs. A-B") IF stain for the stromal markers Pdgfr-α (green) and Pdgfr-β (red) in E18.5 lungs. C) Quantification of the frequency of Pdgfr-α cells as a proportion of all live cells by flow cytometry in E18.5 lungs. Bars represent mean ±SD, n=5 (+/+), 6 (+/-), 11 (-/-).

D-E') IF stain for VE-Cad (green), Pdgfr-β (red), and E-Cad (white) to examine pericyte-EC interaction. F-G') IF stain for the broad EC marker VE-Cad (green). H-I") IF stain for Emcn (green), Claudin-5 (red), and Sox17 (white) to differentiate arterial and venous differentiation. A = artery, V = vein, Br = bronchi/bronchiole. J-K') IF stain for the lymphatic marker Lyve1 (red) and Emcn (white). L-M') IF stain for VE-Cad (green), Sm22a (magenta), and E-Cad (white). Scale bar = 50 μm (A-B",D-E',H-M'), 25 μm (F-G').

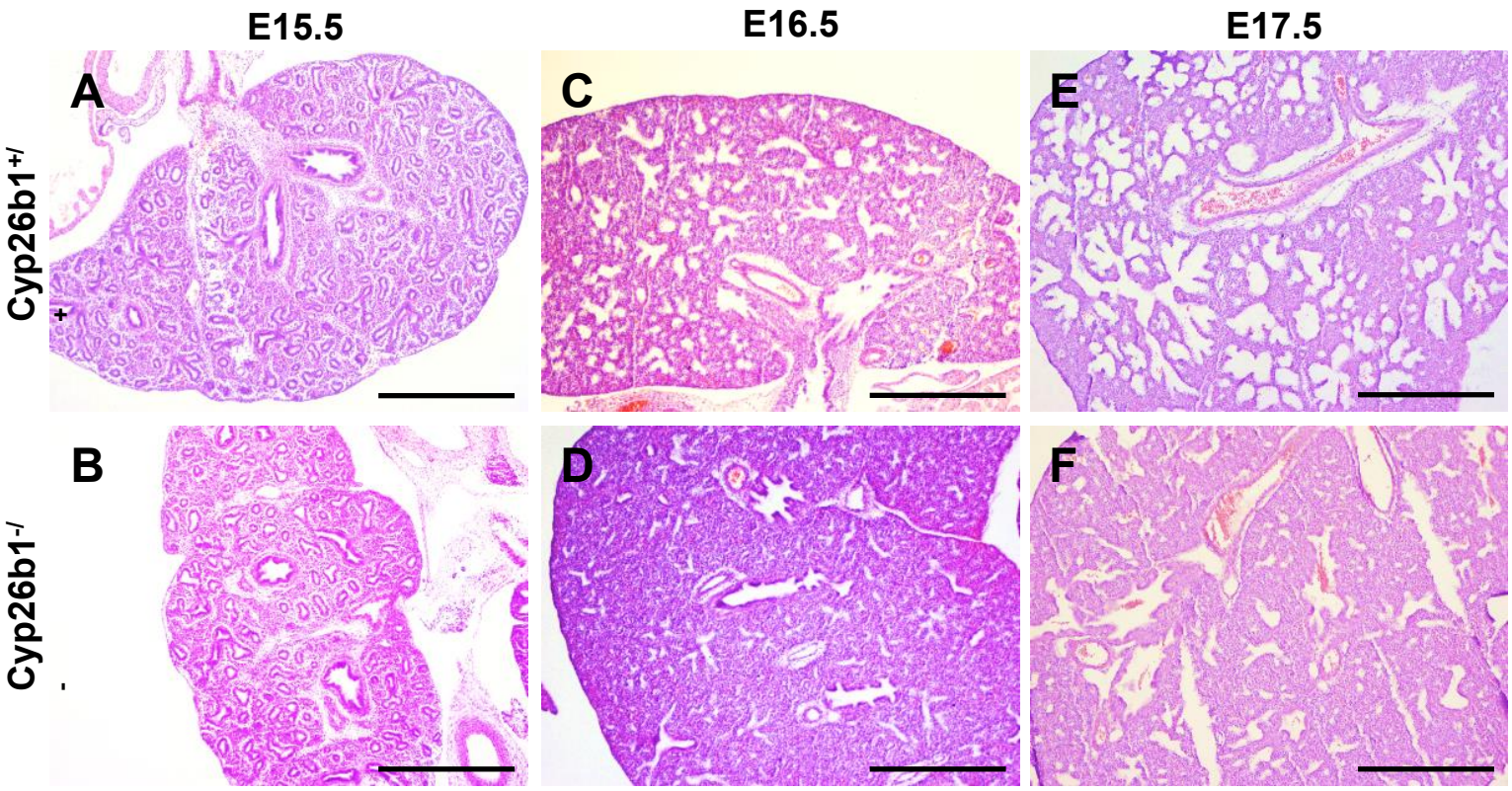

Figure S7. Gross histology of Cyp26b1$^{-/-}$ lungs in late gestation. A-F) H&E stains of Cyp26b1$^{+/+}$ (A, C, E) and Cyp26b1$^{-/-}$ (B, D, F) lungs at E15.5 (A-B), E16.5 (C-D), and E17.5 (E-F). Scale bar: 500 μm.

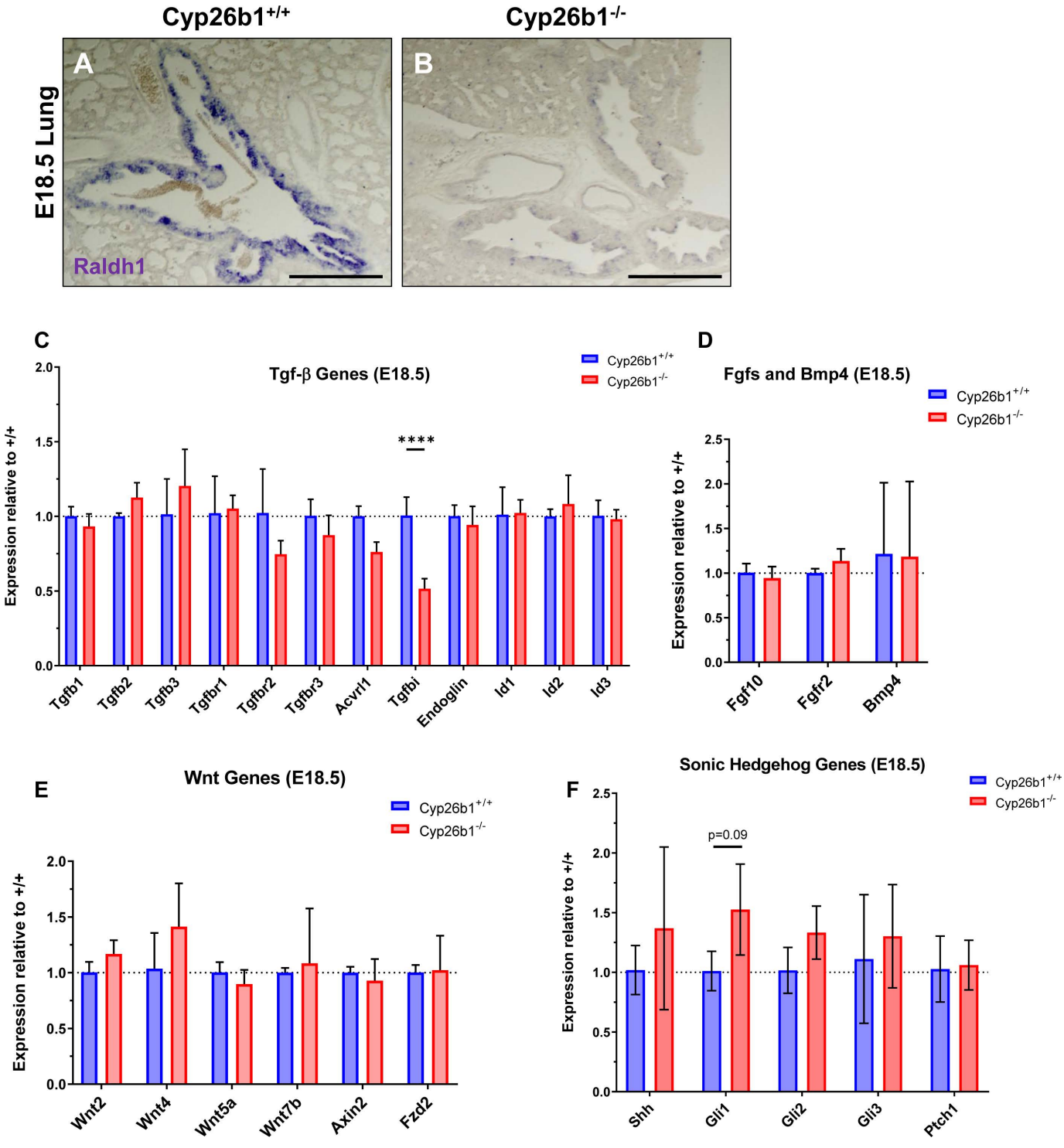

Figure S8. Other signaling pathways implicated in lung development are unaffected in Cyp26b1$^{-/-}$ lungs. A-B) ISH for Raldh1 in E18.5 Cyp26b1$^{+/+}$ (A) and Cyp26b1$^{-/-}$ (B) lungs. C) qRT-PCR for members of the Tgf-β signaling pathway standardized to the expression of +/+ samples for each gene. Bars represent mean ±SD, n=3. Significance was determined using two-way ANOVA with Sidak multiple comparison test on the ΔΔCt values. ****P<0.0001. D) qRT-PCR for established regulators of lung branching, *Fgf10*, *Fgfr2*, and *Bmp4,*standardized to the expression of +/+ samples for each gene. Bars represent mean ±SD, n=6. Significance was determined using two-way ANOVA with Sidak multiple comparison test on the ΔΔCt values. E) qRT-PCR for members of the Wnt signaling pathway standardized to the expression of +/+ samples for each gene. Bars represent mean ±SD, n=4. Significance was determined using two-way ANOVA with Sidak multiple comparison test on the ΔΔCt values. F) qRT-PCR for members of the Shh signaling pathway standardized to the expression of +/+ samples for each gene. Bars represent mean ±SD, n=7 (*Shh,Gli1,Gli2*), 3 (*Gli3,Ptch1*). Significance was determined using two-way ANOVA with Sidak multiple comparison test on the ΔΔCt values. Significance was determined using two-way ANOVA with Sidak multiple comparison test. ****P<0.0001. Scale bar: 500 μm.

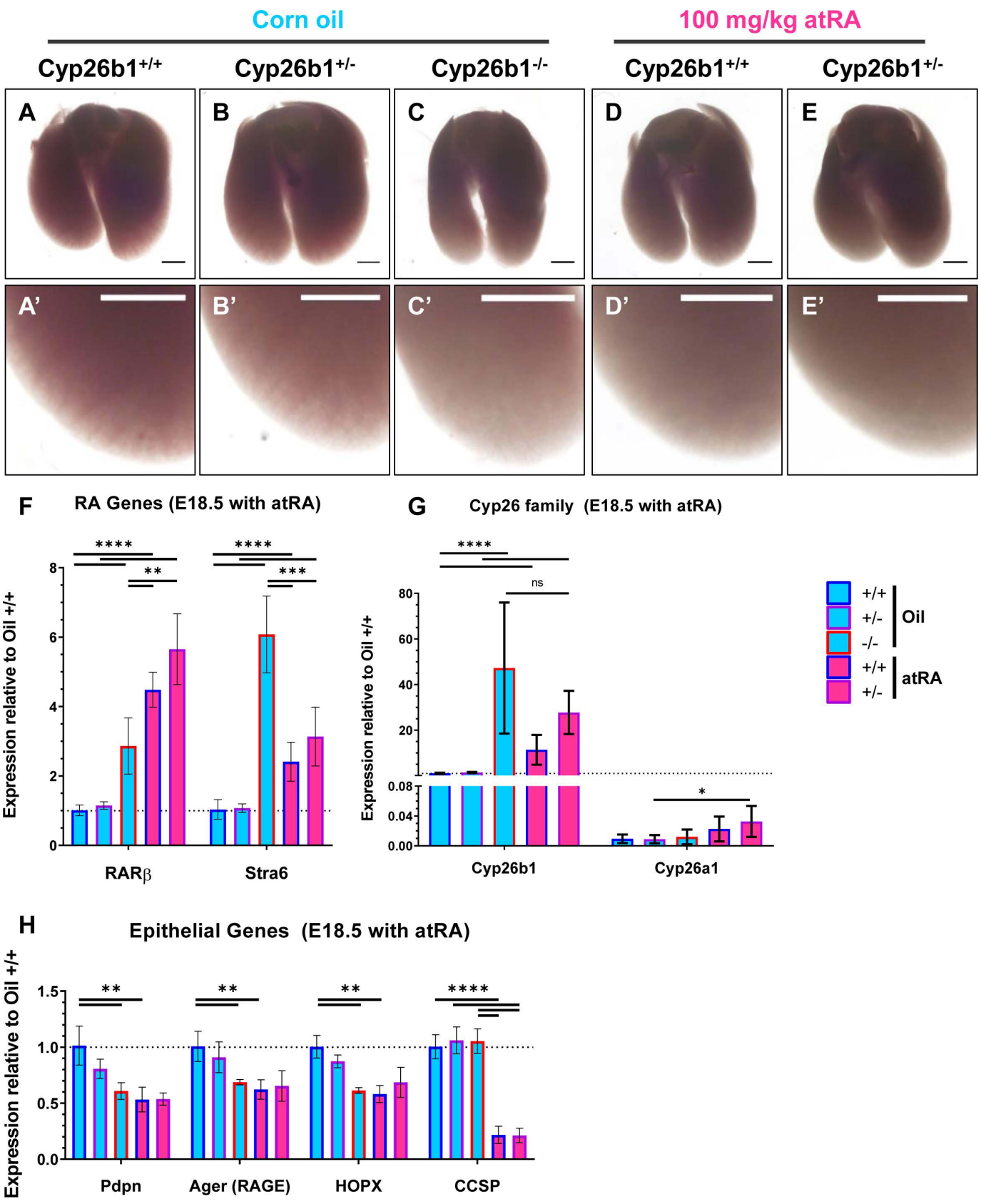

Figure S9. Morphologic and transcriptional changes in RA and epithelial genes with atRA treatment. A-E') Lungs from E18.5 control (A-C) and atRA-treated (D-E) Cyp26b1$^{+/+}$, Cyp26b1$^{+/-}$, and Cyp26b1$^{-/-}$ lungs at time of dissection. Magnified views of the left lobe are shown in A', B', C', D', and E' to highlight loss of distal airspaces in Cyp26b1$^{-/-}$ and atRA-treated Cyp26b1$^{+/+}$ and Cyp26b1$^{+/-}$ lungs. Scale bar = 1 mm. F) qRT-PCR for *RARβ* and *Stra6* standardized to the expression of +/+ samples for each gene. Outline color corresponds to genotype (blue = Cyp26b1$^{+/+}$, purple = Cyp26b$^{+/-}$, red = Cyp26b1$^{-/-}$) and fill color corresponds to treatment group (cyan = control, magenta = atRA). Bars represent mean ±SD, n=3 (oil -/-), 4 (oil +/-), 5 (atRA +/-), 6 (oil +/+, atRA +/+). Significance was determined using two-way ANOVA with Sidak multiple comparison test on the ΔΔCt values. ***P*<0.01, ****P*<0.00 ,*****P*<0.0001. G) qRT-PCR for *Cyp26b1* and *Cyp26a1* following the same coloring scheme in F standardized to the expression of +/+ samples for each gene. Bars represent mean ±SD, n=3 (oil -/-), 4 (oil +/-), 5 (atRA +/-), 6 (oil +/+, atRA +/+). Significance was determined using two-way ANOVA with Sidak multiple comparison test on the ΔΔCt values. **P*<0.05, *****P*<0.0001. H) qRT-PCR for the epithelial genes *Pdpn*, *Ager*, *HOPX*, and *CCSP* following the coloring scheme in F standardized to the expression of +/+ samples for each gene. Bars represent mean ±SD, n=3 (oil -/-), 4 (oil +/-), 5 (atRA +/-), 6 (oil +/+, atRA +/+). Significance was determined using two-way ANOVA with Sidak multiple comparison test on the ΔΔCt values. ***P*<0.01, *****P*<0.0001.

Table S1. List of Primers

sgRNAs	
Cyp26b1_E3-M2	CACACGCACGGCCATTCGGA
Cyp26b1_E6-B2	TCCGGGTGGCCAGCTCGAAG

Genotyping		
Primer Name	**Sequence**	
CK3-F_3bp	AGGCCCAGCGACTTACCACC	WT Band = 724 bp
Cyp26b1_Exon6-LP3	TCGGACAGGTAAGTGGACCT	KO Band = 429 bp
Cyp26b1_Exon6-RP3	TATACTGCAGCTCAACCGGC	

Cyp26b1-KO1-F	CCAGCGACTTACCTTCCGAA	For WT allele = 531 bp
Cyp26b1-KO1-F3bp	AGGAGGCCCAGCGACTTTGG	For KO allele = 528 bp
Cyp26b1_Exon3-R	TGGTCATCTCCTTGCCATGT	

qRT-PCR	
Primer Name	**Sequence**
Cyp26b1_RT-F	ACATCCACCGCAACAAGC
Cyp26b1_RT-R	GGGCAGGTAGCTCTCAAGTG
Cyp26a1_RT-F	CCGGCTTCAGGCTACAGA
Cyp26a1_RT-R	GGAGCTCTGTTGACGATTGTT
Sftpc_RT-F	GGTCCTGATGGAGAGTCCAC
Sftpc_RT-F	GATGAGAAGGCGTTTGAGGT
Pdpn_RT-F	GCCAGTGTTGTTCTGGGTTT
Pdpn_RT-R	TCTCCTGTACCTGGGGTCAC
Sox9_RT-F	GACAAGCGGAGGCCGAA
Sox9_RT-R	CCAGCTTGCACGTCGGTT
Ager_RT-F	GGGAAGAGGGGCAGACAG
Ager_RT-R	TGATGTTCTGACCACCAGCTAC
Aqp5_RT-F	TAACCTGGCCGTCAATGC
Aqp5_RT-R	GCCAGCTGGAAAGTCAAGATT
HOPX_RT-F	ACCACGCTGTGCCTCATC
HOPX_RT-R	GCGCTGCTTAAACCATTTCT
Lamp3_RT-F	GCTGTACTCTTCCTGTCCCTGA
Lamp3_RT-R	CTGTTCTGCTGATGTTGCAGT
Raldh1_RT-F	GCCATCACTGTGTCATCTGC
Raldh1_RT-R	CATCTTGAATCCACCGAAGG
Raldh2_RT-F	CATGGTATCCTCCGCAATG
Raldh2_RT-R	GCGCATTTAAGGCATTGTAAC
Raldh3_RT-F	AACCTGGACAAAGCACTGAAG
Raldh3_RT-R	AATGCATTGTAGCAGTTGATCC
RARa_RT-F	GTGCCATCTGCCTCATCTG
RARa_RT-R	CAGCATGTCCACCTTGTCTG
RARb_RT-F	AGCCCACCAGGAAACCTT
RARb_RT-R	GTCAGCGCTGGAATTCGT

RARg_RT-F	TGACAAGTCTTCTGGCTACCAC
RARg_RT-R	TCTGAATGCTGCGTCTGAAG
Rbp1_RT-F	TAGACGACCGCAAGTGCAT
Rbp1_RT-R	TCTCCCTTCTGCACACACTG
Rbp4_RT-F	AGACACGGAGGCTGGTGA
Rbp4_RT-R	GGCCTGCTTTGACAGTAACC
Crabp2_RT-F	TTGAGGAAATGCTAAAAGCTCTG
Crabp2_RT-R	TCCTGTTTGATCTCGACTGCT
Stra6_RT-F	TCAGGATCCTAAGATCTACAAGCA
Stra6_RT-R	TCAGGAATCCAAGACCCAGA
Dhrs3_RT-F	ATGTTCCAGGGCATGAGAGT
Dhrs3_RT-R	TCCTCCGGGCTACTGTCTC
Cyp26c1_RT-F	GCGCACCTTTGAACTGGA
Cyp26c1_RT-R	ATGCGTGTCTCGGATGCTAT
Cyp26b1_E4-5-F	ACGCCCTGGACATTCTCA
Cyp26b1_E4-5-R	AGATCAACTCCAGGGTTCCA
Ret_RT-F	CAAACTCTATGGCATGTCAGACC
Ret_RT-R	ATCGGCTCTCGTGAGTGGTA
Egr1_RT-F	GTCAGCAGCTTCCCGTCT
Egr1_RT-R	TGAAAGACCAGTTGAGGTGCT
Foxa1_RT-F	GAACAGCTACTACGCGGACA
Foxa1_RT-R	CGGAGTTCATGTTGCTGACA
Pbx1_RT-F	GCCAATATTTATGCTGCCAAA
Pbx1_RT-F	ACATGTTAAAAGAACTGGAAGAACC
Tgfb1_RT-F	TGGAGCAACATGTGGAACTC
Tgfb1_RT-R	GTCAGCAGCCGGTTACCA
Tgfb2_RT-F	AGGAGGTTTATAAAATCGACATGC
Tgfb2_RT-R	TAGAAAGTGGGCGGGATG
Tgfb3_RT-F	CCCTGGACACCAATTACTGC
Tgfb3_RT-3	TCAATATAAAGGGGGCGTACA
Tgfbr1_RT-F	GCAGCTCCTCATCGTGTTG
Tgfbr1_RT-R	AGAGGTGGCAGAAACACTGTAAT
Tgfbr2_RT-F	CCATGGCTCTGGTACTCTGG
Tgfbr2_RT-R	ATGGGGGCTCGTAATCCTT
Tgfbr3_RT-F	TGGCTGTGGTACTAGACATAGGAG
Tgfbr3_RT-R	GGAGCCTGCACCACAATAG
Acvrl1_RT-F	ACACCCACCATCCCTAACC
Acvrl1_RT-R	TGGGGTACCAGCACTCTCTC
Tgfbi_RT-F	GAGCTGCTTATCCCAGATTCA
Tgfbi_RT-R	GGCAGTGGAGACGTCAGATT
Endoglin_RT-F	CATTGCACTTGGCCTACGA
Endoglin_RT-R	GATGTTGACTCTTGGCTGTCC
Id1_RT-F	GCGAGATCAGTGCCTTGG
Id1_RT-R	CTCCTGAAGGGCTGGAGTC
Id2_RT-F	GACAGAACCAGGCGTCCA
Id2_RT-R	AGCTCAGAAGGGAATTCAGATG
Id3_RT-F	GAGGAGCTTTTGCCACTGAC
Id3_RT-R	GCTCATCCATGCCCTCAG

Fgf10_RT-F	GATTGAGAAGAACGGCAAGG
Fgf10_RT-R	GTTGCTGTTGATGGCTTTGA
Fgfr2_RT-F	ATCTGCCTGGTCTTGGTCAC
Fgfr2_RT-R	CTTCTCGGTGTTGGTCCAGT
Bmp4_RT-F	GCCAACACTGTGAGGAGTTTC
Bmp4_RT-R	CACCTCATTCTCTGGGATGC
Wnt2_RT-F	CAGAGATCACAGCCTCTTTGG
Wnt2_RT-R	GCGTAAACAAAGGCCGATT
Wnt4_RT-F	CTCCCTGTCTTTGGGAAGGT
Wnt4_RT-R	TCTCCAGTTCTCCACTGCTG
Wnt5a_RT-F	TGAAGCAGGCCGTAGGAC
Wnt5a_RT-R	AGCCAGCACGTCTTGAGG
Wnt7b_RT-F	GAACTCCGAGTAGGGAGTCG
Wnt7b_RT-R	GTCACAGCCACAATTGCTCA
Axin2_RT-F	CCATGACGGACAGTAGCGTA
Axin2_RT-R	GCCATTGGCCTTCACACT
Fzd2_RT-F	CCGCTCTTCGTATACCTGTTC
Fzd2_RT-R	CGGATGCGGAAGAGTGACA
Shh_RT-F	TCCACTGTTCTGTGAAAGCAG
Shh_RT-R	GGGACGTAAGTCCTTCACCA
Gli1_RT-F	AGGAATTCGTGTGCCATTG
Gli1_RT-R	TCCGACAGCCTTCAAACG
Gli2_RT-F	TGAAGGATTCCTGCTCGTG
Gli2_RT-R	GAAGTTTTCCAGGACAGAACCA
Gli3_RT-F	CATTCCAATGAGAAACCGTATG
Gli3_RT-R	GAGCTGGGGTCTGTGTAACG
Ptch1_RT-F	GCTCTGGAGCAGATTTCCAA
Ptch1_RT-R	ACCCAGTTTAAATAAGAGTCTCTGAAA
Cyclophilin_RT-F	GGAGATGGCACAGGAGGAA
Cyclophilin_RT-R	GCCCGTAGTGCTTCAGCTT

Table S2. Antibody List

Antibody	Company	Catalog Number	Use	Concentration
Aqp5	Abcam	ab78486	IF / WB	1:100 (IF) / 1:1000 (WB)
β-actin	Cell Signaling Technologies	3700	WB	1:2000
β-Galactosidase	Abcam	ab9361	IF	1:100
CCSP	Millipore	07-623	IF	1:100
Claudin-5	Santa Cruz	sc-28670	IF	1:100
E-Cadherin (rat)	Thermo Fisher Scientific	13-1900	IF	1:400
E-Cadherin (mouse)	BD Transduction	610182	IF	1:200
Endomucin	Santa Cruz	sc-65495	IF	1:200
Foxj1	Invitrogen	14-9965-82	IF	1:100
Phospho-Histone H3	Millipore	06-570	IF	1:200
Hopx	Santa Cruz	sc-398703	IF	1:100
Lamp3 (DC-Lamp)	Novus	DDX0191P-100	IF	1:100
Lyve1	Abcam	ab14917	IF	1:100
Nkx2.1	Cell Signaling Technologies	12373s	IF	1:100
Pdgfrα	R&D Systems	AF1062	IF	1:100
Pdgfrβ	Cell Signaling Technologies	3169	IF	1:100
PECAM	BD Pharmingen	553370	IF	1:200
Podoplanin	DSHB	8.1.1	IF	1:100
proSP-C	Millipore	AB3786	IF / WB	1:200 (IF) / 1:2000 (WB)
Sm22a	Abcam	ab14106	IF	1:100
Sox2	Santa Cruz	sc-365823	IF	1:100
Sox9	Millipore	AB5535	IF / WB	1:200 (IF) / 1:2000 (WB)
Sox17	R&D Systems	AF1924	IF	1:100
VE-Cadherin	R&D Systems	AF1002	IF	1:200
CD45-FITC	BD Pharmingen	553080	FC	1:100
CD31-APC	BD Pharmingen	551262	FC	1:200
Sca1 (Ly-6a)-APC-Cy7	BD Pharmingen	590654	FC	1:100
EpCam-PE-Cy7	BioLegend	118216	FC	1:200
CD140a-FITC	Thermo Fisher	11-1401-82	FC	1:50

IF = Immunofluorescence, WB = Western Blot, FC = Flow Cytometry